scientific reports

Check for updates

OPEN

Statistical optimization of eco-friendly synthesized silver nanoparticles using *Discopodium penninervium Hochst* leaf extract for enhanced antimicrobial efficacy

Abreham Mulugeta Getachew✉, Ebise Getacho Bacha & Wondwosen Sime Geleta

Infectious diseases caused by pathogenic microorganisms are a significant global threat, affecting millions of people. The aim of this study was optimizing the eco-friendly synthesis of silver nanoparticles (AgNPs) using *Discopodium Penninervium Hochst* leaf extract via a response surface methodology approach. The ANOVA results revealed that the quadratic model ($p < 0.0001$) was sufficient to achieve the most precise prediction of particle size ($R^2 = 0.995$). A minimum AgNPs size of 21.65 nm, was achieved under optimal conditions. The ultraviolet-visible (UV-vis) UV-vs spectroscopy of the synthesized AgNPs revealed a strong absorption peak at 402 nm. The X-ray diffraction (XRD) analysis confirmed a face-centered cubic crystal structure with average crystallite size of 17.60 nm. Dynamic light scattering (DLS) value (38.62 nm) displays AgNPs was in the nanoscale whereas the zeta potential value (-14.20 mV) indicates its stability. The scanning electron microscopy (SEM) image showed spherical in shape and exhibited an average particle size of 2 µm with some agglomeration. Fourier transform infrared spectroscopy (FTIR) spectra depicted the presence of functional groups from plant extract, which used as a capping agent and bioreduction process. thermogravimetric analysis (TGA) measurement suggested that AgNPs exhibit good thermal stability. The AgNPs exhibited good antimicrobial activities against Gram-negative (*Escherichia coli*) and Gram-positive (*Staphylococcus aureus)* bacteria, as well as fungus (*Candida albicans*) with corresponding inhibition zones of 25 mm (mm), 21 mm, and 20 mm, respectively. The phytochemical screening revealed the presence of bioactive components such as phenols, alkaloids, flavonoids, tannins, steroids, and terpenoids. This study presented rapid, simple, and eco-friendly methods for synthesizing AgNPs with potential antimicrobial applications.

Keywords Discopodium penninervium hochst, Green nanotechnology, Eco-friendly synthesis, Central composite design, Response surfsce methodology, Silver nanoparticles, Antimicrobial activity

Infectious diseases caused by pathogenic agents such as bacteria, viruses, and fungi are a major global hazard, impacting millions yearly[1]. To solve this issue, researchers are investigating a new solution and approaches, such as the synthesis of novel and efficient nanomaterials as an alternative to conventional antibiotics. The production and manipulation of materials in nanometers is the focus of the developing field of nanotechnology in modern science and technology. It also has different medical and biomedical application including the synthesize of nanoparticles and carbon nanotube for bio-imaging, cancer treatment, drug delivery, and antimicrobial purposes[2]. In comparison to bulk substances of the same compositions, nanomaterials display unique physicochemical properties due to possessing a high surface area-to-volume ratio[3]. The main reason for the widespread application of nanoparticles in medicine is their size similarity feature (nanoscale range), which enables them to easily interact with cell membranes, receptors, proteins, and nucleic acids[4]. Through its numerous applications in biomedicine, environmental remediation, renewable energy, and nanomaterial synthesis, green nanotechnology has become a well-known and promising scientific area for environmental sustainability[5]. In order to preserve the health and integrity of diverse ecosystems, it places a strong emphasis

School of Chemical Engineering, Jimma Institute of Technology, Jimma University, P.O. BOX 378, Jimma, Ethiopia. ✉email: abrehammulugeta12@gmail.com

on the application of eco-friendly techniques and environmentally sustainable materials to achieve a balance between economic, social, and environmental issues[6]. Therefore, nanoparticles have become increasingly significant in scientific research due to their extensive applications in medicine, optics, energy, antimicrobial, and catalysis. Metal nanoparticles like silver, copper, and zinc exhibit inhibitory effects on microorganisms. Among them, silver nanoparticles (AgNPs) have gained a promising option due to their strong antimicrobial activities against a broad range of pathogenic microorganisms, including fungi, yeast, and bacteria[7]. AgNPs have remarkable properties such as surface plasma response (SPR), biocompatibility, high surface area to volume ratio, and high stability[8]. These properties make them suitable for various applications, including antibacterial and antifungal activities[9], cancer treatment and drug delivery[10], corrosion resistance, and biosensors[11], and catalysis[12]. In recent years, AgNPs have been confirmed to serve as a non-toxic and safe inorganic antimicrobial agent, effectively eradicating approximately 650 different disease-causing microorganisms[13].

Over the years, physical and chemical methods like the sol-gel process, co-precipitation, microwave-assisted synthesis, pulsed laser ablation, electrochemical synthesis, ultrasonication, and chemical reduction of metallic salt have been used to synthesize AgNPs[14]. However, there has been a recent surge in the synthesis of AgNPs using plants and microorganisms, such as bacteria and fungi[15]. Compared to other methods, green synthesis is preferred for commercial production due to its simplicity, efficiency, scalability, and environmentally friendly nature[16]. Additionally, the plant-mediated synthesis of AgNPs is gaining popularity because it eliminates the need for cell culture maintenance and poses no biohazard risk[14]. Despite using natural reducing agents and being environmentally friendly, green production of nanoparticles has some drawbacks. Plant extracts contain a complex variety of biomolecules which makes the size and shape of the nanoparticles vary[17].

Discopodium Hochst represents a unique African genus within the Solanaceae family and is largely available and easily accessible in Ethiopia. *Discopodium Penninervium Hochst* locally known as "Ameraro" in the Amharic language. It is a medical plant, predominantly found in Ethiopia, Cameroon, Uganda, and parts of central Africa. Medicinal plants are one of the most significant global sources for developing novel medications[18]. *Discopodium penninervium* Hochst is an ethnomedicinal plant traditionally used in Ethiopia for treating wounds, fever, and microbial infections[19]. Its therapeutic efficacy is attributed to a rich composition of bioactive phytochemicals, including alkaloids, flavonoids, tannins, phenolics, tepenoids, and saponins and biologically, the plant has the antimicrobial and antioxidant properties. These secondary metabolites not only account for the plant's medicinal value but also play a critical role in the green synthesis of nanoparticles by acting as reducing, capping, and stabilizing agents[20]. Hence, the phytochemical abundance and ethnopharmacological relevance of *Discopodium penninervium* justify its selection as a sustainable and effective source for nanoparticle synthesis with enhanced biological activity. Nowdays the researcher use this plant for the synthesis of AgNPs aimed at remediating infectious microorganisms.

Response Surface Methodology (RSM) is a statistical technique used to optimize processes by exploring the relationships between various factors and desired outcomes. It involves designing experiments, building a mathematical model based on the results, and then using the model to identify the optimal combination of factors that will yield the best results. This study employed central composite design (CCD) as an RSM optimization method to investigate the effect of independent variables on the green synthesis of AgNPs. The reaction temperature, pH, and concentration of silver nitrate were independent factors, while particle size was a dependent variable.The adequacy of this model is subsequently validated through analysis of variance (ANOVA)[21].

Extensive researches have been conducted on the preparation of silver nanoparticles using different plant extracts such as *Pisonia Alba*[22], *Lallemantia royleana*[23] *Moringa oleifera*[24] *Azadirachta. indica* (Neeem)[25], *Trigonella. foenum-graecum* (Fenugreek)[26] and *Citrullus colocynthis* (Bitter Apple)[27], *Capsicum frutescens* (sweet pepper)[28], *Pongamia pinnata*[29] *Cinnamon zeylanicum* bark[30]. In addition, previous studies have predominantly employed the one-factor-at-a-time (OFAT) strategy to optimize process variables in the synthesis of AgNPs. However, this method is both time-consuming, and resource-intensive, and it fails to adequately capture the intricate interrelationships between parameters[31]. *Discopodium penninervium Hochst* is employed for the first time as reducing and stabilizing agent in the environmentally friendly synthesis of nanoparticles, so the present study, introduce a novel green synthesis of silver nanoparticles using Discopodium penninervium Hostchs leaf extract. The phytochemical composition of this plant plays an important role in reducing and stabilizing silver ions during the formation of nanoparticles. Moreover, this work implies a Central Composite Design (CCD) under Response Surface Methodology (RSM) to optimize basic synthesis parameters making different from many previous studies that used trial and error approaches. The synthesized AgNPs also shows strong and broad-spectrum antimicrobial activities against Gram-positive, Gram-negative bacteria and fungus. Therefore, this study provides a new plant-base route and a statistically optimized green methods that advances suitable nanomaterial development.

Thus, this study aimed to develop novel AgNPs through a green synthesis approach using a leaf extract from *Discopodium Penninervium Hochst* as a green reducing agent and to optimize the synthesis process, the influence of pH, silver nitrate ($AgNO_3$) concentration, and reaction temperature on the particle size was investigated using the RSM-CCD. The synthesized AgNPs were characterized using various analytical techniques including Ultraviolet-visible (UV-vis) spectroscopy, X-ray diffraction (XRD), Fourier Transform Infrared spectroscopy (FTIR), Dynamic Light Scattering (DLS), Scanning Electron Microscopy (SEM), and Thermogravimetric Analysis (TGA). Finally, the antibacterial and antifungal activities of the synthesized AgNPs were evaluated against Gram-positive (*Bacillus cereus* and *Staphylococcus aureus*), Gram-negative (*Escherichia coli* and *Salmonella typhi*) bacteria, and the pathogenic fungus (*Candida albicans*).

Materials and methods

Materials

In this study, analytical grade chemicals and reagents were utilized. Silver nitrate ($AgNO_3$, 99.5% purity), Ferric chloride ($FeCl_3$, 99% purity), Hydrochloric acid (HCl, 35.5% purity), Sulfuric acid (H_2SO_4, 98% purity), Sodium hydroxide (NaOH, 99% purity), Mercury chloride ($HgCl_2$, 98% purity), Muller Hint agar nutrient (CM0337B), and potassium iodide (KI, 89.0% purity) were purchased from (LOBA CHEMIE PVT.LTD., India).

Experimental procedure

Plant collection and identification

A mature Discopodium peninervum leaf was freshly collected from Jimma Institute of Technology, Jimma, Ethiopia, located 352 km southwest of Addis Ababa ($7°41'6N$ and $36°49'53$ E) in Autumn season. The leaves were washed with double distilled water to remove impurities. The formal identification of *Discopodium penninervium Hochst* undertaken by Zemede Asfaw, et[32]., 26] Addis Ababa University. A voucher specimen has been deposited in the National Herbarium (ETH) Addis Ababa University, under deposition number AT65. All experimental research studies in volving Discopodium penninervium Hochst were conducted were conducted in compliance with institutional, national, and international guidelines. The collection of plant material adhered to the IUCN Policy Statement on Research Involving Species at Risk of Extinction and the Convention on International Trade in Endangered Species of Wild Fauna and Flora (CITES)[34].

Preparation of plant extract

The extraction of *Discopodium Penninervium Hochst* leaf extract was prepared using the method described with a minor modification[35], as shown in Fig. 1. The mass 20 of gram (g) of the washed leaves were chopped into small pieces using a knife, and the chopped leaves were placed in a 500 milliliter (mL) glass beaker with 200 mL of double-distilled water. The mixture was stirred vigorously and heated on hotplate (HSC-19T, TX, USA) at 60 °C for 10 min (min). The extract was then filtered through Whatman No. 1 filter paper, and the clear filtrate was then stored in a refrigerator at $4°C$ for succeeding experiments.

Phytochemical screening of Discopodium penninervium Hochst leaf extract

The leaf extract of *Discopodium Penninervium Hochst* was subjected to initial phytochemical analysis to identify secondary metabolites, using a slightly modified procedure of the established method used by[36].To test for saponins, 0.2 mL of the extract was manually agitated with 5 mL of double distilled water and heated to boiling point on a hotplate (HSC-19T, TX, USA) at 100 °C. For flavonoids, 3 mL of the extract was treated with 1 mL of a 10% sodium hydroxide (NaOH) solution. Phenols were tested by adding 1 mL of the leaf extract to 2 mL of an aqueous ferric chloride ($FeCl_3$) solution. Terpenoids and steroids were tested by mixing 5 mL of the Discopodium peninervum leaf extract with 2 mL of chloroform and 3 mL of concentrated sulfuric acid (S_2HO_4). For tannin, 0.5 mL of the Discopodium peninervum leaf extract was mixed with 1 mL of double distilled water and 2 drops of $FeCl_3$ solution. Alkaloids were tested by adding 2 mL of the Discopodium peninervum leaf extract to Wagner's reagent and a drop of hydrochloric acid (HCl). Consequently, the presence of those phytochemicals was confirmed based on color intensity, foam formation, and precipitation. To confirm the validity of the phytochemical screening of Discopodium penninervium Hochst leaf extract, various standard compounds were employed as positive controls, including gallic acid for phenols, catechin for tannins, quercetin for flavonoids, reserpine for alkaloids, and a saponin standard for saponins. Distilled water served as the negative control[37].

Phytochemical determination of Discopodium penninervium Hochst leaf extract

The quantitative phytochemical of *Discopodium Penninervium Hochst* leaf extract was determined using a method adopted by[38] with slight modification.

Determination of flavonoids The 3 g of the sample was extracted with 50 mL of 80% aqueous methanol at room temperature. The mixture was filtered through a Whatman No. 1 filter paper into a pre-weighted 250 mL beaker. The extract from filtrate was evaporated to dryness in a water bath, and the final weight was measured.

Determination of alkaloids The 1.5 g of the sample was weighed into a 250 mL beaker, and 200 mL of 10% acetic acid in ethanol was added. The mixture was left to stand for 4 h (h), after which it was filtered. The filtrate was concentrated in a water bath to reduce its volume to one-quarter of the original. Concentrated ammonium

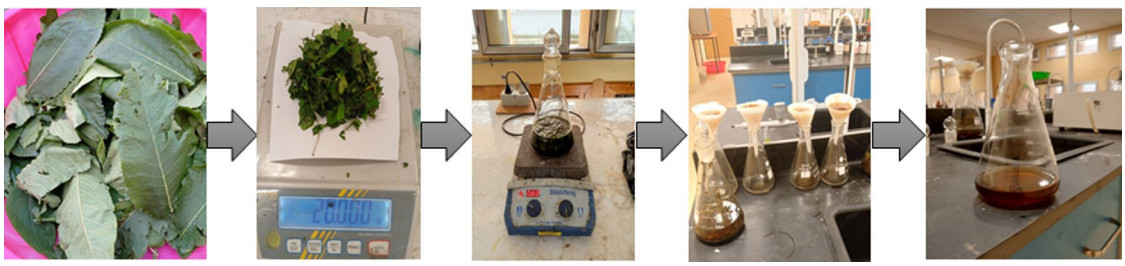

Fig. 1. Extraction of *Discopodium Penninervium Hochst* leaf extract.

hydroxide (NH_4OH) was then added dropwise until precipitation was complete. The solution was allowed to settle, and the resulting precipitate was collected and dried. The residue was weighed, which is alkaloids.

Determination of tannins The 3 g of the ground sample was measured into a conical flask, and 100 mL of 2 M hydrochloric acid (HCl) was added. The mixture was heated in a water bath for 30 min. The extract was cooled and filtered using Whatman No. 1 filter paper. The filtrate was extracted twice with 40 mL of diethyl ether. The ether extract was evaporated in a water bath to dryness, and the residue was weighed.

Proximate analysis of discopodium penninervium Hochst leaf

The proximate composition of *Discopodium Penninervium Hochst* leaves was analyzed using the standard methods prescribed by the Association of Official Analytical Chemists (AOAC)[39]. The compositions including moisture content, Ash content, volatile matter, and fixed carbon were determined.

Moisture content (MC): To determine the MC, 10 g of *Discopodium Penninervium Hochst* leaf was dried in an oven at $105^{\circ}C$ until the constant weight was reached. The MC was calculated by using Eq. (1).

$$\mathrm{MC} = \left(\frac{\mathrm{W_1} - \mathrm{W_2}}{\mathrm{W_1}}\right) 100\% \tag{1}$$

where W_1 represents the weight of sample before drying and W_2 the weight of the sample after drying.

Ash content (AC): The 10 g of the *Discopodium Penninervium Hochst* leaf was fired in furnace at 700 °C for 30 min to determine the AC. The total AC of the sample was determined by using Eq. (2).

$$AC = \left(\frac{W_2}{W_1}\right) 100\% \tag{2}$$

where W_2 represents the weight of the sample after firing and W_1 represents the weight of the sample before firing.

Volatile matter (VM): A 10 g sample of *Discopodium Penninervium Hochst* leaf was heated in an oven at 105 °C for 1 h. to remove the moisture content. The heated leaf was then burned in a furnace 925 °C for 7 min to measure the VM. The VM was calculated using Eq. (3).

$$\mathrm{VM} = \left(\frac{\mathrm{W_2} - \mathrm{W_3}}{\mathrm{W1}}\right) 100\% \tag{3}$$

where W_1 is the weight before heating, W_2 after heating, and W_3 after burning.

Fixed carbon (FC): The mass balance for the sample *Discopodium Penninervium Hochst* leaf was used to determine the FC content. FC was determined using **Eq. (4)**.

$$FC\% = 100\ \% - (\mathrm{MC} + \mathrm{AC} + \mathrm{VM}) \tag{4}$$

Synthesize of silver nanoparticles (AgNPs)

The green synthesis of AgNPs (Fig. 2) followed a method by[40] with a slight modification. 0.026 g of silver nitrate ($AgNO_3$) was dissolved in 100 mL of double distilled water in a glass beaker and stirred slowly with a magnetic stirrer for 30 min. After stirring, 30 mL of *Discopodium Penninervium Hochst* leaf extract was added to the $AgNO_3$ solution. Then, 1 mol of sodium hydroxide (NaOH) solution was added to adjust the pH to 11.

The solution was heated to 90 °C for 1 h until its color changed from clear white to reddish-brown, indicating the formation of AgNPs. Subsequently, the solution was centrifuged at 2000 rpm for 10 min and washed several times with double distilled water to remove any unreacted substances, impurities or excess reagents. The paste was dried in an electric oven at 110 °C, calcinated in an air furnace at 200 °C for 6 h, and stored in a desiccator for subsequent characterization and experimentation.

Optimization of process parameters

The most important step in the synthesis of nanoparticles is optimizing the process parameters to produce smaller and more stable particles. Response surface methodology (RSM) has been frequently used for optimizing an important component in the synthesis of biomolecules[41]. This study employed central composite design (CCD) as an RSM optimization method to investigate the effect of independent variables on the green synthesis of AgNPs. The reaction temperature, pH, and concentration of silver nitrate were independent factors, while particle size was a dependent variable. AgNPs have been synthesized from plant leaf extract at temperatures ranging from 25 to 95 °C[42–45]. Therefore, in this research, a low level (−1) was considered as 60 °C and a high level (+ 1) as 90 °C (Table 1). The alkaline pH range significantly increased the reduction and stabilization potential of plant extract in AgNP synthesis[46]. Hence, for this study, a pH of 8 was employed as low level (−1), while a pH of 12 was employed as high level (+ 1). The most common silver salt concentration is 1 mM, although the concentration levels of 0.1–10 mM and 0.5–2.5 mM were also reported by the previous study[47]. However, silver agglomeration became more pronounced when the concentrations of $AgNO_3$ exceeded 10 mM[48]. Consequently, for this study, 1.5 mM was selected as the low level (−1) and 5 mM as the high level as detailed in Table 1.

The total number of experimental runs was calculated using Eq. (5)[49].

$$\mathrm{N} = 2^{\mathrm{n}} + 2\mathrm{n} + \mathrm{n_c} \tag{5}$$

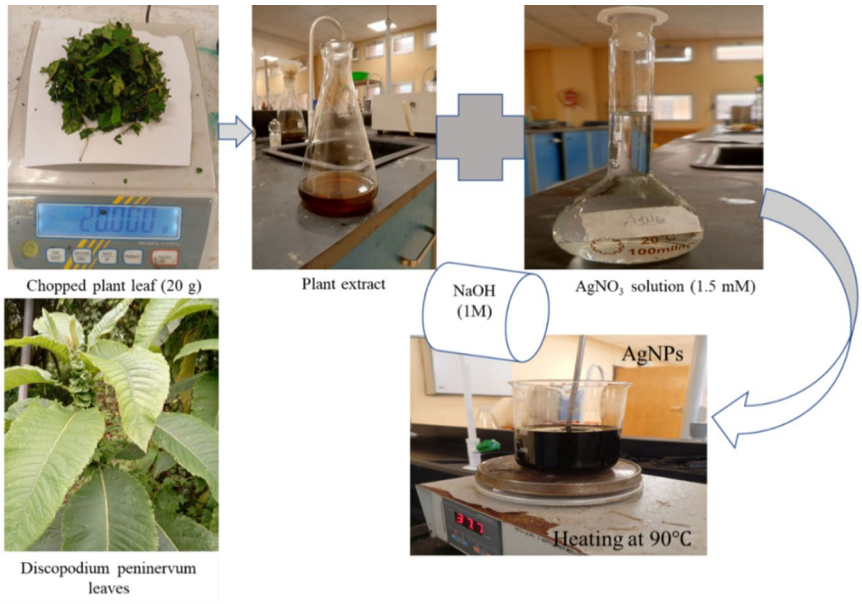

Fig. 2. Synthesis of silver nanoparticles (AgNPs).

Independent Variables	Code	Level				
		- α	−1	0	+1	+α
Reaction Temperature ($^{\circ}C$	A	49.7731	60	75	90	100.227
pH level	B	6.63641	8	10	12	13.3636
Concentration of $AgNO_3$ (mM)	C	0.06863	1.5	3.25	5	6.19314

Table 1. The design of experimentation for the independent variables.

Where N is the total number of runs, n is the number of independent variables, and the terms 2^n, 2n, and n_c are the factorial runs, axial runs, and center runs, respectively. In this study, a total of 20 experimental runs were conducted, consisting of 8 cube poins, 6 replications at the center pont, and 6 axial points for the three independent variables tabluted in Table 1. The relationship between the components and the response was determined by utilizing the quadratic model equation presented in Eq. (6).

where Y represents the particle size of AgNPs, which is the response variable. The term β0 stands for the regression coefficient that represents the intercept; βi, βii, and βij correspond to the linear, quadratic, and interaction coefficients, respectively. The independent variables are represented by Xi and Xj, and ε denotes the error term[50].

Model validation

The validity of the optimized parameters was evaluated using standard deviation (SD) to measure variability and mean absolute percentage error (MAPE) to assess prediction accuracy Eqs. (7 and 8)[51].

$$Y = \beta 0 + \sum_{i=1}^{k} \beta iXi + \sum_{i=1}^{k} \beta iixi^2 + \sum_{i=1}^{k-1} \sum_{j=1}^{k} \beta ijXiXj + \varepsilon \tag{6}$$

$$\mathrm{SD} = \sqrt{\sum \frac{(\mathrm{xi} - \mathrm{x}^{-})^2}{\mathrm{n} - 1}} \tag{7}$$

where, xi represents the actual value, x^- is the mean of actual values, and n is the number of experimental runs.

$$\mathrm{MAPE} = \frac{100 \times \sum \left| \frac{\mathrm{xactual} - \mathrm{xpredict}}{\mathrm{xactual}} \right|}{\mathrm{n}} \tag{8}$$

Material characterization

UV- visible spectrophotometer analysis

UV-visible absorption spectroscopy (PerkinElmer Lambda 25, Massachusetts, USA) at a wavelength of 200–700 nm was employed to analyze the characteristic absorption peak of the synthesized AgNPs. The energy band gap of the synthesized AgNPs was calculated by Tauc's formula shown in Eq. (9)[52].

$$(\alpha\, \mathrm{hv})^{\mathrm{n}} = \mathrm{A}\,(\mathrm{hv} - \mathrm{E_g}) \tag{9}$$

where hv is photon energy, α is the absorption coefficient, A is constant, E_g is the energy band gap, and n is either 2 for direct transformation or ½ for indirect transformation.

X-ray diffraction (XRD) analysis

X-ray diffractometer (XRD, Drawell XRD-7000, China) was used to determine the crystalline size and crystallinity of greenly synthesized AgNPs, and the average crystalline size was computed using the Debye-Scherrer formula Eq. (10)[53].

$$D = \frac{k\lambda}{\beta\, \cos} \tag{10}$$

where D is the mean crystalline size, k is the Scherrer's constant (shape factor) with a value of 0.9, λ is the X-ray wavelength = 0.15406, β is the full width at half maximum (FWHM) in radian, and is the Bragg angle.

Fourier transform infrared (FTIR) analysis

The functional groups involved in the synthesized AgNPs were determined using the Fourier transform infrared spectrum (FTIR, PerkinElmer Spectrum Two, Massachusetts, USA) in the wavenumber range of 4000–400 cm^{-1} with a resolution of 4 cm^{-1}.

Dynamic light scattering (DLS) and zeta potential analysis

Average crystallite size and zeta potential analysis were carried out by DLS (Malvern Analytical, UK).

Scanning electron microscopy (SEM)

The surface morphology of the synthesized AgNPs was studied using scanning electron microscopy (SEM, SHIMANDZU, Brno) with a voltage of 15 kV.

Thermogravimetric analysis (TGA)

The thermal stability of AgNPs was assessed with a thermal analyzer model DTG-60 H (SHIMADZU, Japan) across a temperature range of 0 to 800 $^{\circ}C$ at a heating rate of 10$^{\circ}C$/min under an inert nitrogen (N_2) atmosphere.

Antibacterial and antifungal activities

The antibacterial and antifungal properties of AgNPs were assessed using the agar disc diffusion method[54]. Bacterial and fungal samples for this study were obtained from a microbiology research laboratory, at Jimma University, Ethiopia. AgNPs were tested against gram-positive (*Bacillus cereus* and *Staphylococcus aureus*), gram-negative (*Escherichia coli* and *Salmonella typhi*), and pathogenic fungus (*Candida albicans*). Pure cultures of the test organisms were first subcultured on nutrient agar and incubated at 37 °C for 24 h to obtain fresh colonies. A loopful of each bacterial culture was then transferred into 5 mL of nutrient broth and incubated at 37 °C with shaking at 20 rpm 18 h to reach the logarithmic growth phase. The bacteria were cultured on Muller Hinton agar (MHA) and fungi on potato dextrose agar (PDA). The pure colonies were transferred to tubes containing a sterile normal saline solution (0.85%NaCl) and mixed to agust its tubidity at the McFarland standard solution. Then sterile filter paper disks, 6 mm in diameter, were placed on a Petri dish containing agar media. AgNPs were dissolved in dimethyl sulfoxide (DMSO) at concentrations of 50, 25, 6.25, 3.125, and 1.5625 milligram per milliliter (mg/mL). DMSO served as a negative control, while gentamicin and clotrimazole were used as positive control bacteria and fungi, respectively. The inhibition zone for each bacterial and fungal strain was measured in mm after the plates were incubated for 24 h at 37 °C and the minimum inhibition concentration (MIC) was determined by comparing the concentration at which growth started to the control.

Results and discussions

Phytochemical characterization of *Discopodium penninervium Hochst* leaf extracts

A qualitative phytochemical screening was performed on *Discopodium Penninervium Hochst* leaf extract to identify various phytochemicals present in the leaves of this plant.The existence of these phytochemicals was confirmed by observing changes in color, foam formation, and precipitation. The phytochemical properties of the *Discopodium Penninervium Hochst* leaf extract were summarized in Table 2; Fig. 3.

The result confirmed the presence of bioactive compounds such as alkaloids, tannins, saponins, phenols, flavonoids, terpenoids, and steroids in the leaf extract. The presence of bioactive compounds may contribute a significant role to the reduction, capping, and stabilization of AgNPs[36].

Phytochemical characterization of *Discopodium penninervium Hochst* leaf extracts

The quantitative analysis of primary metabolites indicated the presence of various phytochemical constituents in the leaf extract of *Discopodium Penninervium Hochst.* The test was performed by triplicate measurements, and

No⁻	Phytochemical Compounds	Tests/Reagents	Observation	Results
1	Tannins	Ferric chloride test	Blue-black color	+
2	Alkaloids	Mayer's reagent	Cream precipitate	+
3	Saponins	Frosting test	Frothing	+
4	Phenols	Ferric chloride test	Black color	+
5	Flavonoids	Alkaline reagent test	Intense yellow color	+
6	Terpenoids	Salkowski test	The reddish-brown color at the interface	+
7	Steroids	Salkowski test	The red color at the lower surface	+

Table 2. Bioactive phytochemical analysis of *Discopodium penninervium Hochst* leaf extract. (+) indicates the presence of bioactive compounds.

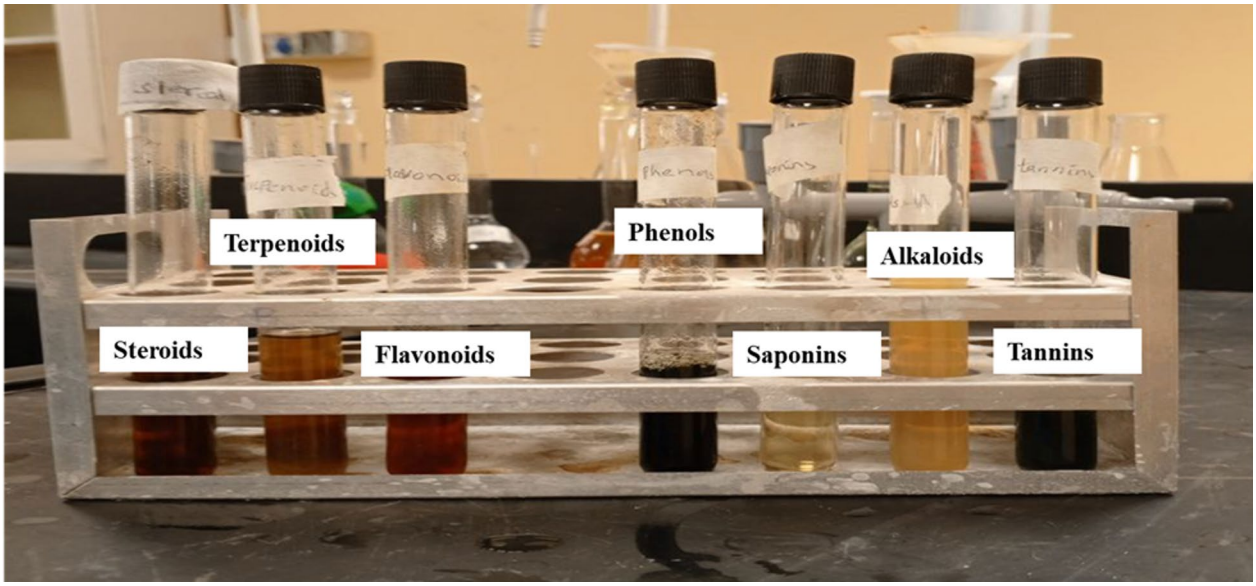

Fig. 3. Bioactive phytochemical screening of *Discopodium Penninervium Hochst* leaf extract.

No⁻	Phytochemicals	Quantity (W/m)
1	Alkaloids	6.94 ± 0.31
2	Flavonoids	18.182 ± 1.02
3	Tannins	2.42 ± 0.52

Table 3. Quantitative phytochemical determination of *Discopodium penninervium Hochst* leaf extract.

the mean values are presented along with their standard deviations, as detailed in Table 3. The extract contained 6.94 ± 0.31 W/m of alkaloids, 18.182 ± 1.02 W/m of flavonoids, and 2.42 ± 0.52 W/m of tannins.

Proximate analysis of *Discopodium penninervium Hochst* leaves

The proximate analysis of *Discopodium peninervum* leaves, as shown in Fig. 4, provides valuable insights into their suitability for nanoparticle synthesis. The relatively low moisture content (4.3%) suggests minimal interference from water during the synthesis process, which can enhance nanoparticle stability[55]. The ash content (14.5%) indicates the presence of inorganic components that may contribute to the formation of bioactive nanoparticles[56]. The high volatile matter (60.3%) suggests a rich composition of organic compounds, which could act as reducing and stabilizing agents during AgNP synthesis[57]. Additionally, the fixed carbon content (29.9%) may influence the structural integrity of the synthesized nanoparticles, potentially enhancing their stability and functionality[58].

Design of experiment and statistical analysis

Experimental design

CCD-RSM methodology was used to optimize the synthesis of silver nanoparticles (AgNPs) using different process parameters (reaction temperature, pH, and concentration of silver nitrate), which affect the dependent

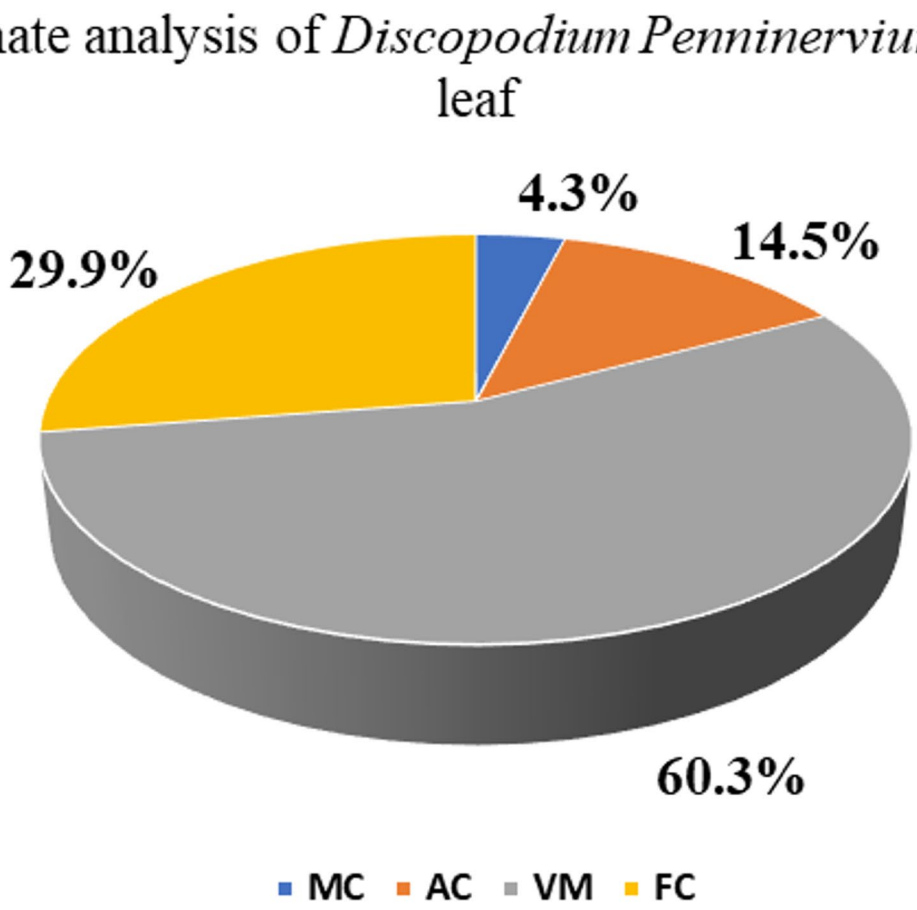

Fig. 4. Moisture content, ash content, volatile matter, and fixed carbon content of *Discopodium Penninervium Hochst* leaves.

variables (response). The design matrix generated by the Design Expert consists of 20 experiments, including predicted and actual values with obtained results in Table 4.

Model fit statistics (ANOVA)

The analysis of variance (ANOVA) results provide information on the importance of the model terms. The model F-value of 219.70 implies that the model is significant, as indicated in Table 5. A high F-value of 219.70 indicates that the possibility of obtaining such a large F-value by chance is extremely low, with only 34.29% chance. A P-value less than 0.05 indicates that the model terms are significant[59]. In this case, A, B, C, A^2, B^2, and C^2 are significant model terms. The values greater than 0.1 indicate that the model terms are not significant. As a result, all interactions, squares, and linear terms significantly impact AgNPs synthesis.

On the other hand, the Lack of Fit F-value of 1.46 suggests that the lack of fit is not significant compared to the pure error. There is only a 34.29% lack of fit F-value this great might occur due to noise. A non-significant lack of fit indicates that the model is very near to perfect fitness[60].

Additionally, the model's suitability was assessed using the coefficient of determination (R^2) value in Table 6, which indicates the extent to which variability in the green synthesis of AgNPs can be explained by the model. A higher R^2 value suggests a better fit between expected and observed data[61]. The R^2 value of 0.995 indicates that the model can explain 99.50% of the variability in the green synthesis process. Furthermore, the adjusted R^2 value of 0.99 and the predicted R^2 value of 0.97 were computed. These values suggest a satisfactory match between observed and predicted values. The other important statistic is adequate precision, which determines the signal-to-noise ratio, which should generally be more than 4 according to[62]. The appropriate precision was determined to be 47.97, indicating that the signal-to-noise ratio is sufficient for navigating the design area.

Model fit summary

The detailed model fit summary of RSM is shown in Table 7. The result revealed the R^2 values of the linear and quadratic models were 0.7333 and 0.995, respectively. The lower R^2 value of 0.7333 for the linear model indicates that it captures a moderate amount of variance but may fail to adequately account for complex relationships in the data. In contrast, the much higher R^2 value of 0.995 for the quadratic model suggests a near-perfect fit, demonstrating its higher capability to model the relationship between the independent and dependent variables.

Std	Run	Factor 1 A: Temperature ($^{\circ}C$)	Factor 2 B: pH	Factor 3 C: Concentration of $AgNO_3$ (mM)	Response Particle size (nm)	Predicted value (nm)
14	1	75	10	6.19	117.98	121.35
6	2	90	8	5	99.99	98.91
7	3	60	12	5	89.95	87.14
20	4	75	10	3.25	34.53	37.24
15	5	75	10	3.25	35.98	37.24
12	6	75	13.36	3.25	35.6	38.61
18	7	75	10	3.25	34.48	37.24
16	8	75	10	3.25	38.38	37.24
3	9	60	12	1.5	25.74	26.03
2	10	90	8	1.5	43.74	45.77
4	11	90	12	1.5	21.55	20.78
1	12	60	8	1.5	64.08	65.69
17	13	75	10	3.25	40.88	37.24
9	14	49.7731	10	3.25	73.75	73.92
10	15	100.23	10	3.25	63.49	64.43
19	16	75	10	3.25	39.38	37.42
8	17	90	12	5	98.18	95.78
5	18	60	8	5	104.94	104.93
11	19	75	6.64	3.25	76.48	74.58
13	20	75	10	0.31	27.54	25.28

Table 4. Predicted and actual response of the experimented central composite design of AgNPs.

Source	Sum of Squares	Df	Mean Square	F-Value	*P*- Value	
Model	**17381.81**	**9**	**1931.31**	**219.70**	**< 0.0001**	**Significant**
A- Temperature	108.56	1	108.56	12.35	0.0056	
B- pH	1562.58	1	1562.58	177.75	< 0.0001	
C-Concentration	11140.20	1	11140.20	1267.26	< 0.0001	
AB	107.53	1	107.53	12.23	0.0058	
AC	96.67	1	96.67	11.00	0.0078	
BC	239.04	1	239.04	27.19	0.0004	
A^2	1837.21	1	1837.21	208.99	< 0.0001	
B^2	674.87	1	674.87	76.77	< 0.0001	
C^2	2344.42	1	2344.42	266.69	< 0.0001	
Residual	87.91	10	8.79			
Lack of Fit	52.24	5	10.45	1.46	0.3429	Not significant
Pure-error	35.67	5	7.13			
Cor Total	17469.72	19				

Table 5. The ANOVA result of the response surface quadratic model.

St. Dev.	2.96	R^2	0.995
Mean	58.33	Adjusted R^2	0.99
C.V.%	5.08	Predicted R^2	0.97
		Adeq precision	47.97

Table 6. Model accuracy measurement for particle size.

Source	Std. Dev.	R^2	Adjusted R^2	Predicted R^2	PRESS	
Linear	17.06	0.7333	0.6833	0.6208	6623.78	
2FI	18.01	0.7587	0.6474	0.3737	10940.82	
Quadratic	**2.96**	**0.995**	**0.993**	**0.9743**	**449.73**	**Suggested**
Cubic	2.54	0.9978	0.9930	0.9581	723.50	**Aliased**

Table 7. Model fit summary response surface methodology (RSM).

Therefore, quadratic model is suggested for the best determination of the relationship between independent and dependent variables.

Model equation for particle size

The RSM results showed that the particle size ranged from 21.55 to 117.98 nm. Equation (11) expresses the predictive quadratic model equation obtained from multiple regression analysis of experimental data to model the relationship between independent and dependent (response) variables.

$$\begin{aligned} Y = 37.24 - 3.05A - \ 12.15B + 26.89C + 3.67AB + 5.47BC \\ +12.29A^2 \ + 6.84B^2 + 12.75C^2 + ABC + A^2B + A^2C + AB^2 \end{aligned} \tag{11}$$

The parameters' coding values were A for the reaction temperature, B for the pH, and C for the concentration of $AgNO_3$. The coefficients of the coded parameter in the equation indicate the main and interaction effects of each coded factor, along with the impacts of the squared terms. A positive coefficient implies that increasing the coded factor increases the particle size, whereas a negative coefficient suggests that increasing the coded factor decreases the particle size. According to the equation, reaction temperature (A) and pH (B) have negative coefficients. This demonstrates that increasing the A and B factors leads to smaller particle sizes[63]. However, the concentration of $AgNO_3$ (C) shows a positive coefficient. As a result, raising the concentration of $AgNO_3$ yields larger particle sizes[64]. The interaction effect, such as AB, AC, and BC, indicates the combined effects of two factors on the particle size.

Additionally, based on the coefficients of the squared terms (A^2, B^2, and C^2), these factors also influence the particle size[65]. The concentration of $AgNO_3$ and pH have a relatively strong effect on the particle compared to the reaction temperature by considering the magnitude of the coefficient values. In case of cubic model the R^2 value of 0.9978 and adjusted R^2 of 0.993. This indicates that the model can explain 99.780% of the variability. The cubic model shows slightly higher R^2 in comparision with quadratic model. This indicates overfiting due to the additional polynomial term as illuastared in Eq. (12). Therefore, quadratic model was selected as optimal model and minimizing averfitting risk.

$$\begin{aligned} Y = 37.24 - 3.05A - 12.15B + 26.89C + 3.67AB + 5.47BC \\ +12.29A^2 + 6.84B^2 + 12.75C^2 + ABC + A^2B + A^2C + AB^2 \end{aligned} \tag{12}$$

Model diagnostics test

The diagnostic plots were thoroughly evaluated to determine the suitability of the suggested model as shown in Fig. 5**(a-b)**. Figure 5 **(a)** shows a normal probability plot of the residual value, which shows that the residual aligns with a straight line with no significant variance. This indicates the distribution of the errors follows a normal pattern, thus supporting the assumption of normality. Figure 5 **(b)** shows the correlation between experimental and predicted particle sizes. The mathematical model utilized in this study is a second-order polynomial equation that describes the effect of individual variables and interactions. The adequacy of this model was evaluated by plotting and comparing the experimental values against the predicted values of the particle size.

The fitted line plot shows the overall agreement between the result obtained from experimental data and the predicted values. The straight-fitted line suggests a minimal difference and indicates a good agreement between the experimental data and the predicted value.

Effect of single process parameters on the particle size

The Fig. 6**(a-c)** illustrates the influence of three parameters temperature, pH, and silver nitrate concentration ($AgNO_3$) on particle size.

The particle size appears to decrease from 64. 08 nm to 43.74 nm as the temperature increases from $60^\circ C$ to $90^\circ C$ as illustrated in Fig. 6 **(a)**. This trend suggests that higher temperatures may enhance nucleation rates over growth rates, leading to the formation of smaller particles. Increased thermal energy at higher temperatures promotes faster reaction kinetics, resulting the formation of more uniform and smaller particle[66]. The Fig. 6 **(b)** shows that particle size is influenced by pH, as the pH increasing from 8 to 12 particles size decreasing from 64.08 nm to 25.75 nm. This could be due to changes in surface charge or solubility affecting nucleation and growth processes[67]. The particle size increases from 64.08 to 104.94 nm as the concentration of $AgNO_3$ rises from 1.5 to 5 mM as shown in Fig. 6**(c)**. Higher silver ion concentrations provide more material, which leads to larger particles. At lower concentrations, there is less material, so smaller particles are formed[68]. Generally, temperature and pH can be fine-tuned to minimize particle size, while higher concentrations of $AgNO_3$ tend to increase particle size[69].

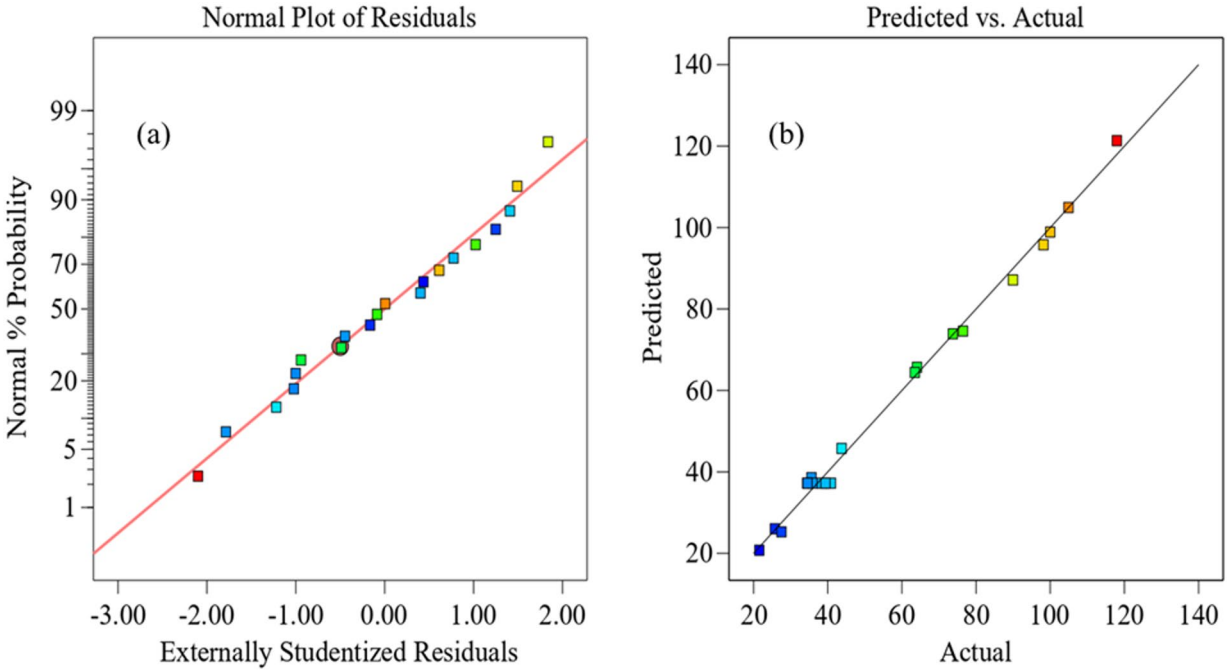

Fig. 5. (**a**) Normal percentage probability of studentized residual and (**b**) actual vs. predicted particle size plot.

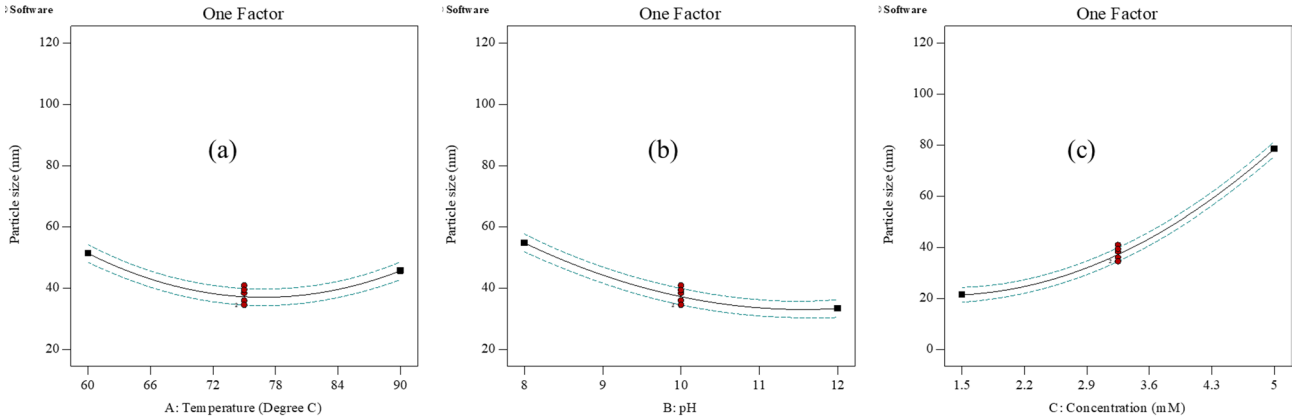

Fig. 6. Effect of temperature(**a**), pH(**b**), and concentration of silver nitrate on particle size.

Interaction effect

The 3D response surface plots indicate the effects of synthesis parameters on particle size. Figure 7**(a-c)** is a surface graph demonstrating how synthesized parameters affect particle sizes. When examined, the impact of the two components on the response value, with one factor remaining constant at the center point. Figure 7 **(a)** shows the effect of reaction temperature and pH on particle size while maintaining the silver nitrate ($AgNO_3$) concentration constant. It has been shown that as both reaction temperature and pH increase, the size of particles decreases. Compared to lower pH ranges, higher pH ranges produce smaller particle sizes, particularly pH ranges 10.2–12. According to[70], a higher pH level results in a smaller particle size.

The interaction effect between reaction temperature and the concentration of $AgNO_3$ is illustrated in Fig. 7 **(b)**. The concentration of $AgNO_3$ and reaction temperature have a negative interaction effect at the center point of pH., The reaction temperature rose from 60 to 90 °C. The particle size slightly decreases as the concentration of $AgNO_3$ solution decreases. According[71], the size of the nanoparticles (NPs) decreases as the temperature rises, which aligns with this study.

The interaction effect of pH and concentration of $AgNO_3$ at a constant reaction temperature is shown in Fig. 7 **(c)**. The concentration of $AgNO_3$ has significant impacts on particle formation and size. High metal precursor concentrations in the reaction mixture can induce NPs to agglomerate, resulting in high particle size.

According to[72], increasing the pH level and decreasing the concentration of precursor results in a smaller particle size, which is in line with this study.

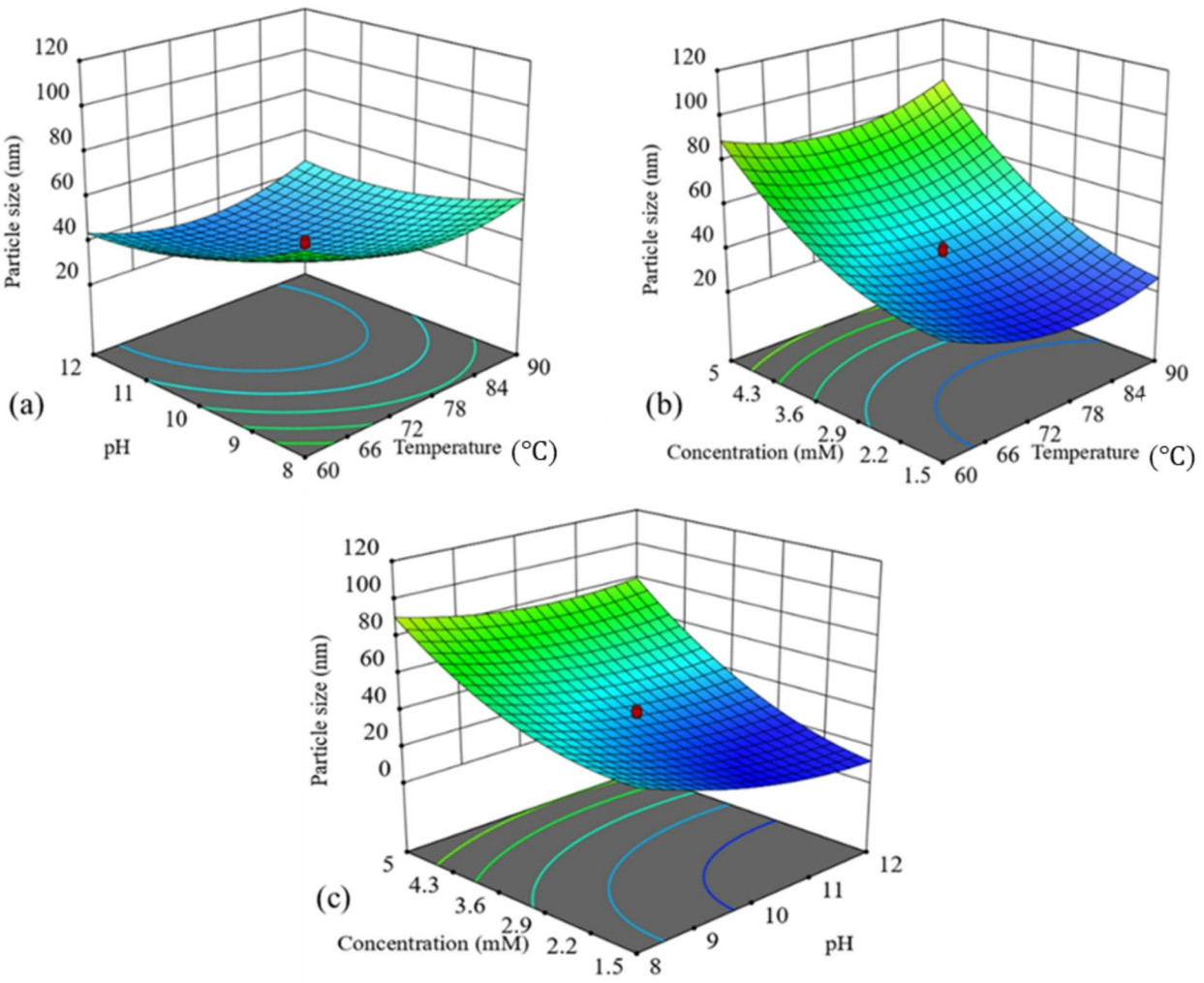

Fig. 7. 3D plots of the interaction effect (**a**) pH and reaction temperature, (**b**) reaction temperature and concentration of $AgNO_3$, (**c**) concentration of $AgNO_3$ and pH.

Optimization of the experimental parameters

Figure 8 shows that the optimal conditions for the process were a reaction temperature of 81.06 ℃, a pH of 11.49, and $AgNO_3$ concentration of 2.13 mM. CCD-RSM analysis of optimized results revealed that the smallest particle size of silver nanoparticles (AgNPs) was 21.65 nm.

Model validation

Triplicate experiments were conducted using the predicted optimal process parameters from the Design Expert software to validate the developed model, as shown in Table 8. The validation analysis showed a standard deviation (SD) of 0.54, a mean absolute percentage error (MAPE) of 3.84%, and an accuracy of 96.16% were calculated.

Material characterization

UV-Vis analysis

The UV-vis spectroscopic study shows the plasmon resonance property and confirms the reduction of metal ions and the formation of nanoparticles. As shown in Fig. 9, the sharp peak of AgNPs was observed at a wavelength of 402 nm, which proves the formation of AgNPs. The presence of a peak in the 300–500 nm range revealed the successful green synthesis of AgNPs, consistent with previous finding[73].

The relationship between hv and $(\alpha\ hv)^2$ is expressed by Tauc's plot (Fig. 10). The Tauc plot generated for the synthesis of AgNPs, as illustrated in Fig. 10, indicated a direct band gap energy of 3.38 eV for AgNPs, which is in agreement with the previous finding[74]. Similar results were reported by[17,62].

XRD analysis

The XRD measurement was carried out to identify the phase purity and crystal structure of the prepared AgNPs[75]. The XRD pattern of the produced AgNPs is illustrated in Fig. 11. As shown in Fig. 11, the XRD pattern

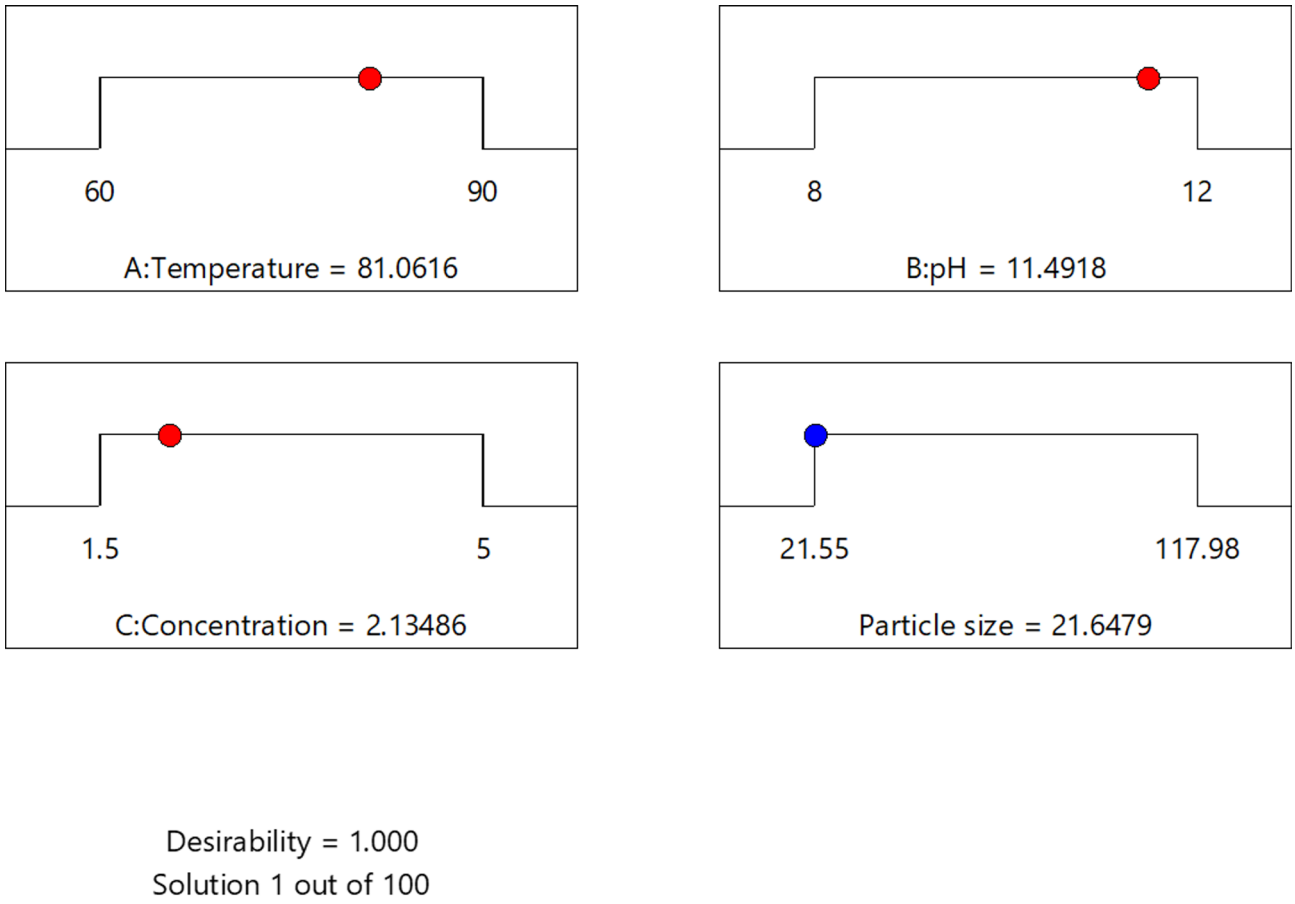

Fig. 8. Optimized ramps for the minimum particle size of silver nanoparticles (AgNPs) by CCD-RSM.

Temperature (℃)	[AgNO3]	pH	Actual Value (nm)	Predicted Value (nm)	SD	MAPE (%)	Accuracy (%)
81.06	2.13	11.5	22.6	21.65			
81.06	2.13	11.5	20.57	21.65			
81.06	2.13	11.5	21.21	21.65	0.54	3.84	96.16

Table 8. Model validation for optimization of silver nanoparticles (AgNPs) particle size.

of the synthesized AgNPs showed a well-defined face-centered cubic (FCC) crystal structure, as revealed by the presence of characteristic peaks at 34.4°, 38.34°, 44.46°, 64.67°, and 77.59°. These peaks correspond to (100), (111), (200), (220), and (311) planes, respectively, which are in agreement with the standard JCPDS card 74–2251[76]. Furthermore, the calculated average crystallite size, as depicted in Table 8, of 17.60 nm is consistent with the previous study. Additionally, the calculated average crystallite size of 17.60 nm, as shown in Table 9, aligns with the findings of a previous study[43] that reported a similar average crystallite size of 20 nm. A few extra unassigned peaks were also observed near the main characteristic peaks, indicating the possible crystallization of a bioorganic layer on the surface of the nanoparticles[77].

FTIR analysis

Fourier transforms infrared spectroscopy (FTIR) analysis is commonly conducted to identify the functional groups involved in *Discopodium Penninervium Hochst* leaves extract and silver nanoparticles (AgNPs). The FTIR spectra of AgNPs and Discopodium peninervum leaf extract were recorded in the range of 400–4000 cm^{-1}, as shown in Fig. 12.

The projecting peaks for AgNPs were observed at 3451.38 cm^{-1}, 1636.36 cm^{-1}, 1381.03 cm^{-1}, 1066.40 cm^{-1}, and 568.38 cm^{-1}. The strong absorption peak at 3458.49 cm^{-1} corresponds to the O −H stretch of alcohols and phenols[78], while the peak at 1636. 36 cm^{-1} is attributed to the C −N bend due to primary amine. The peak at 1381.03 cm^{-1} is assigned to the C −H bending of alkanes, and the peak at 568.38 cm^{-1} corresponds to C −Cl stretching of alkyl halide[79]. This indicate that the AgNPs are well formed and have functional groups that could potentially useful for various application in nanotechnology[80]. In the *Discopodium peninervum* leaf

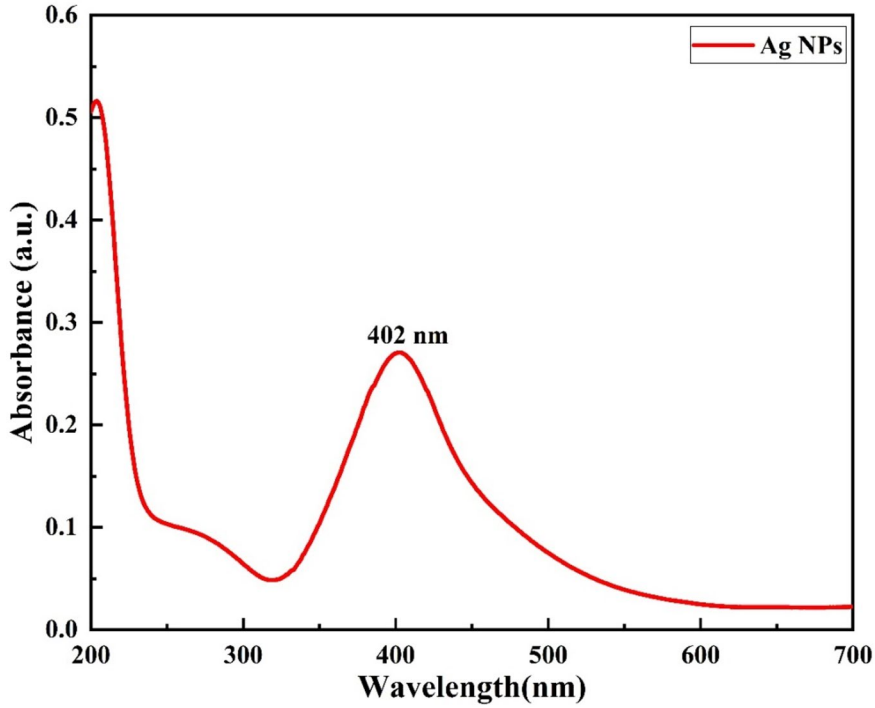

Fig. 9. UV-Vis absorbance spectra of silver nanoparticles (AgNPs).

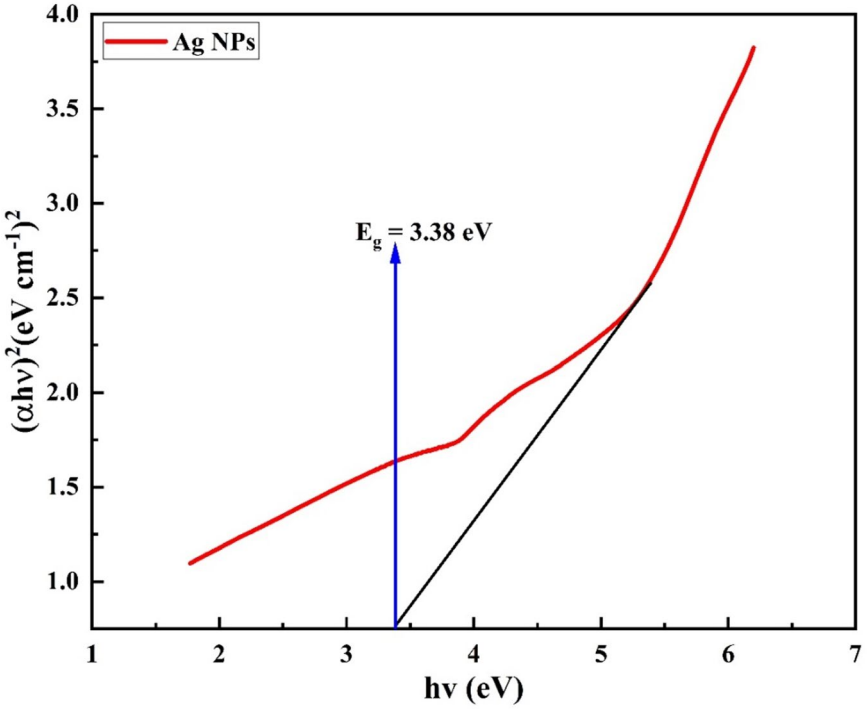

Fig. 10. The energy band gap of silver nanoparticles (AgNPs).

extract, peaks were observed at 3412.65 cm^{-1}, 2068.77 cm^{-1}, 1630.04 cm^{-1}, 1400 cm^{-1}, 1138.34 cm^{-1}, 1059.29 cm^{-1}, 758.10, cm^{-1}, 660.08 cm^{-1}, and 607.11 cm^{-1} These peaks are associated with O −H stretching, alkynes ($C \equiv C$)stretching, C −H stretching due to alkanes, C =C stretching of alkenes, C–O stretching corresponds to vibrations in alcohols, esters, or ethers, which are commonly found in plant-derived biomolecules, phenolic groups, or flavonoids[81], N −O bending due to nitro groups, C −N stretching of alkyl amine, the peak at 758.10

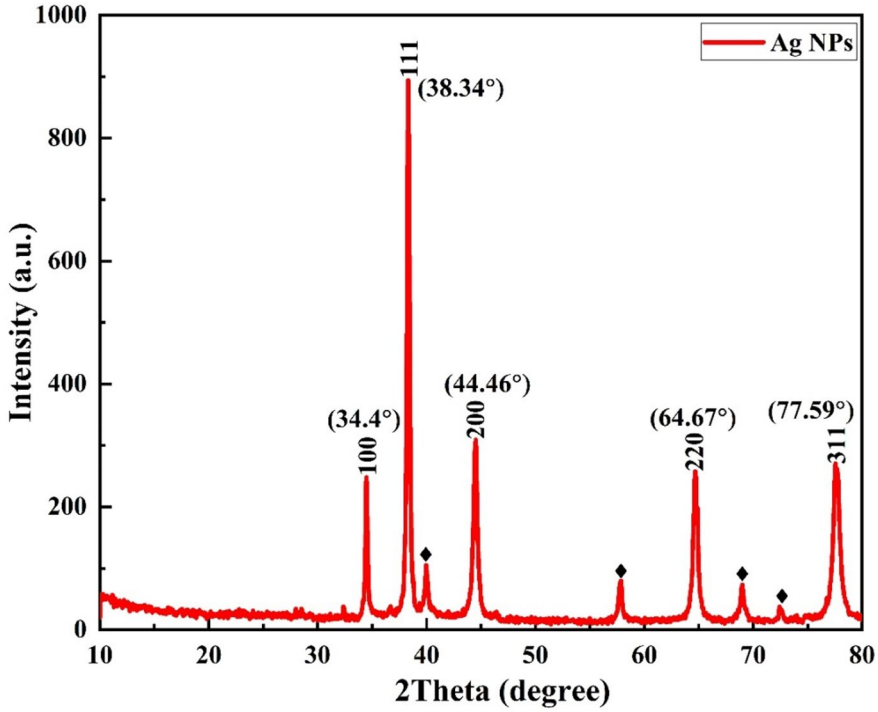

Fig. 11. XRD pattern of silver nanoparticles (AgNPs).

Position 2 θ (°)	FWHM (°)	d -spacing (nm)	Lattice parameter (nm)	Crystallite size
34.40	0.3574	0.23	0.23	23.28
38.34	0.4571	0.26	0.45	18.41
44.46	0.5252	0.21	0.41	16.35
64.67	0.6362	0.14	0.40	14.78
77.59	0.6721	0.12	0.40	15.17
Average crystallite size				**17.60**

Table 9. Physical parameters of silver nanoparticles (AgNPs) calculated from XRD data.

cm^{-1} to 660 cm^{-1} can be attributed to aromatic C-H bending vibrations[82], and C —Br stretching[83], respectively. Therefore, the main functional groups of hydroxyl alcohols, alkanes, amines, alkenes, alkyls, alkynes, and phenols were identified. Similar results were reported by[39,40,60].

DLS and zeta potential analysis

The particle size distribution and zeta potential of the green synthesized silver nanoparticles (AgNPs) were evaluated using Dynamic light scattering (DLS). The synthesis AgNPs exhibited an average size of 38.61 nm (Figs. 13) with a polydispersity index (PDI) of 0.346.

PDI is a measurement of the size distribution of AgNPs from 0.000 to 0.5. PDI greater than 0.5 value indicates the aggregation of particles[84]. Therefore, AgNPs synthesized using *Discopodium Penninervium Hochst* leaf extract exhibit good stability, with no aggregation observed.

Additionally, zeta potential analysis (Fig. 14) and the result revealed a negative surface charge of −14.2 mV, indicating good colloidal stability. Balamurugan et al.[85] reported that AgNPs synthesized by utilizing Elaeocarpus serratus fruit extract have a zeta potential value of −13.9 mV, which is in good agreement with this research. Particles having zeta potential values ranging from + 30 to −30 mV are regarded as being in a stable suspension[86].

SEM analysis

Figure 15 illustrates a SEM micrograph of greenly synthesized AgNPs obtained through the mediation of *Discopodium Penninervium Hochst* leaf extract. The analysis revealed that these synthesized AgNPs have a spherical shape and also show agglomeration. This observation is consistent with a previously reported study[87].

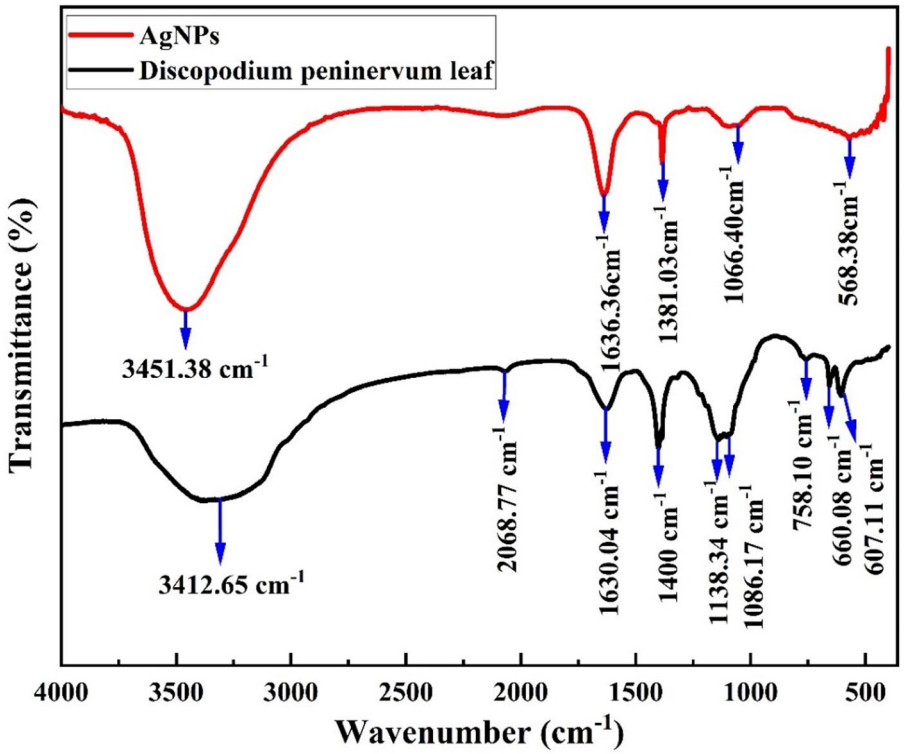

Fig. 12. FTIR graph of silver nanoparticles (AgNPs) and *Discopodium Penninervium Hochst* leaf extract.

TGA analysis

The thermal stability of the biosynthesized silver nanoparticles AgNPs was evaluated using thermogravimetric analysis (TGA) by taking 5.44 milligram (mg) of AgNPs. Figure 16 shows the thermal properties of greenly synthesized AgNPs. TGA analysis revealed three distinct decomposition stages within the temperature range of 0 to 800$^{\circ}C$, with a heating rate of $10^{\circ}C/\mathrm{min}$ under a nitrogen atmosphere. The initial weight loss of 1.7% observed between 161.59 and 327.23$^{\circ}C$ is due to the decomposition of volatile organic compounds and the desorption of surface-adsorbed moisture. The second stage showed a 10.42% weight loss between 327.23 and 466.49$^{\circ}C$ attributed to the decomposition of plant-derived organic biomolecules such as flavonoids, phenolic acids, and carbohydrates adhered to the AgNPs surface[88]. At the third stage, a gradual weight loss of 2.28% was observed between 466.49 and 796.9$^{\circ}C$, probably related to the thermal degradation of oxygen molecules and persistent aromatic compounds on the surface of the AgNPs. The TGA result indicated a total decomposition of 14.4% of the AgNPs due to the desorption of bioactive organic compounds. At a temperature above 800 $^{\circ}C$, the TGA curve showed no weight loss, indicating that the synthesized AgNPs were stable within this temperature range. This is in agreement with the reported decomposition behavior of AgNPs as described by[89].

Analysis of antibacterial and antifungal activities of AgNPs

The antimicrobial activity of AgNPs was evaluated against four bacterial strains: two gram-positive bacteria (*B. cereus* and *S. aureus*) and two Gram-negative bacteria (*E. coli* and *S. typhi*), as well as one fungus (*C. albicans*) by employing the disk diffusion method (Fig. 17). Gentamicin and clotrimazole were used as positives for bacteria and fungi, respectively, while DMSO served as a negative control. The antimicrobial effectiveness of AgNPs against tested bacteria and fungi was confirmed by measuring the result inhibition zone in mm, as shown in Fig. 17. The result, presented in Table 10, indicated that AgNPs exhibited significant antimicrobial activity against all tested bacterial and fungal strains. Notably, the AgNPs exhibited the highest antibacterial activity against *E. coli* and *S. aureus*, with inhibition zones of 25 mm and 21 mm, respectively. Gram-negative bacteria were more sensitive to AgNPs than Gram-positive bacteria, due to their outer layer of lipopolysaccharides and thin peptidoglycan layer, which attract the positively charged AgNPs and facilitate adhesion. In contrast, the thick peptidoglycan layer in Gram-positive bacteria limits the AgNPs' release and uptake of vital cellular components, impairing their function. However, AgNPs can penetrate the cell wall of the bacteria and be effective against both Gram-positive and Gram-negative bacteria[90]. For *C. albicans*, the inhibition zone was 20 mm which is similar to the positive control (clotrimazole), demonstrating the AgNPs efficiently inhibit this pathogenic fungus strain. Minimum inhibition concentration (MIC) is the lowest concentration of antimicrobials that prevent the visible growth of microorganisms[91]. In this study, the MIC AgNPs were determined by using the broth microdilution method as recorded by[92].

The detailed results of the MIC of AgNPs are in Table 10. The result revealed the MICs of the synthesized AgNPs were 0.78, 0.40, 0.07, 1.56, and 0.20 mg/mL for *B. cereus*, *S. aureus*, *S. typhi*, *E. coli*, *and C. albicans*, respectively as shown Fig. 18.

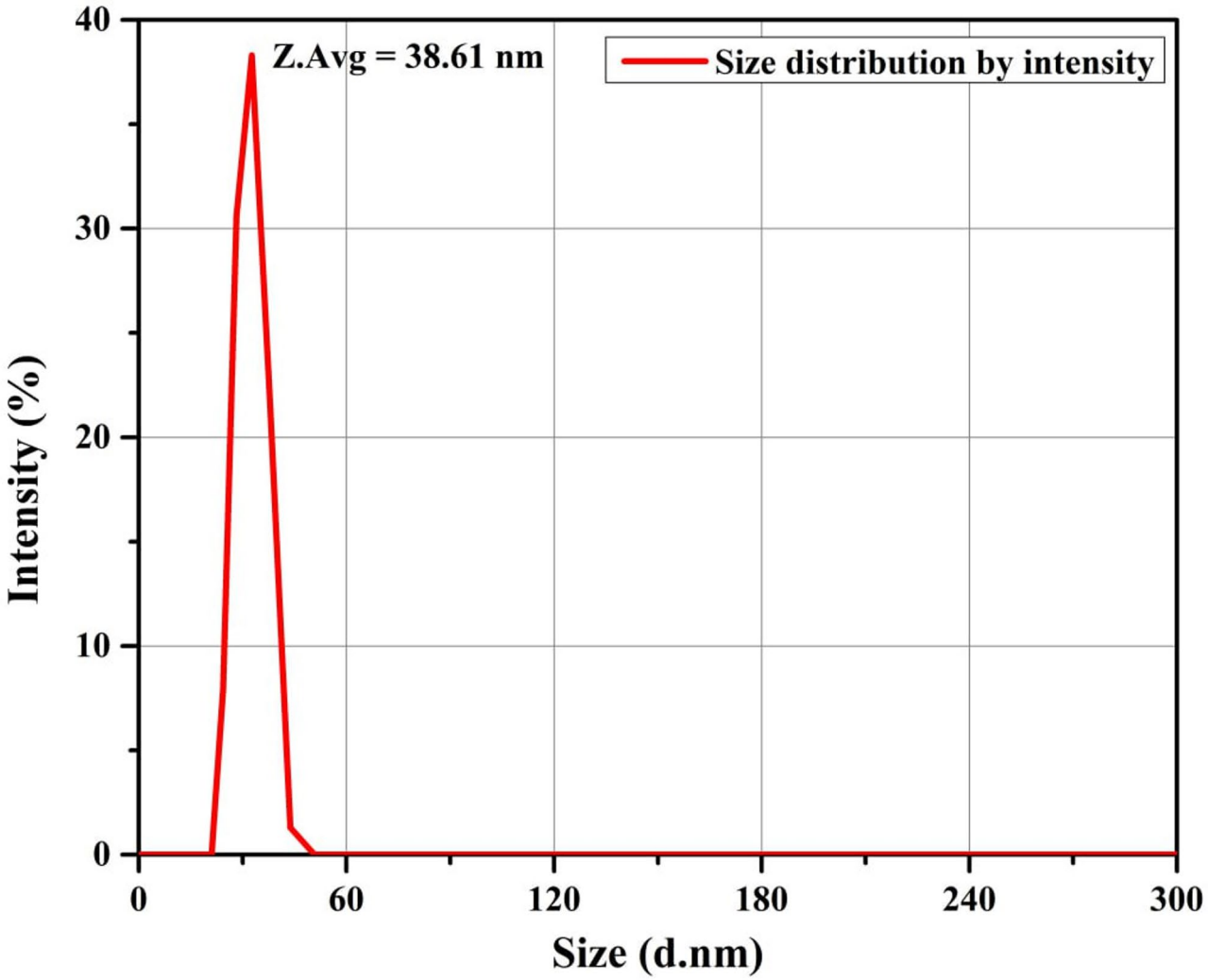

Fig. 13. Particle size distribution graph of silver nanoparticles (AgNPs).

T-tests analysis

The statistical validation of antimicrobial activites of AgNPs were confirmed by t-test. T-test analysis revealed a statistically significant difference between the inhibition zone mean (11.68 mm), and the hypothesized mean (0.2 mm) ($t = 12.41$, $df = 4$, $p = 0.00024 < 0.05$) as indicated in Table 11. This indicates that the synthesized AgNPs exhibited a significant antimicrobial effect against the tased strain.

Mechanism of antimicrobial activities of AgNPs

Reactive oxygen species (ROS) mechanisim of antimicrobial activities of the synthesized AgNPs was illustrated in Fig. 19 below. Reactive oxygen species (ROS) are metabolic byproducts produced by various cells, with the endoplasmic reticulum and mitochondria being key in their production and metabolism[93]. These highly reactive molecules can oxidize cellular structures and biomolecules, leading to DNA damage, protein modifications, and lipid peroxidation, which ultimately cause cell death. AgNPs can generate ROS within cells, resulting in oxidation stress and damage to cellular structure. AgNPs release Ag^{+} ions, which can deactivate vital enzymes by interacting with their thiol groups[94]. When these ions contact bacterial cells, they disrupt essential functions, leading to cell damage. This disruption can generate ROS by inhibiting respiratory enzymes, causing the microbial cell to self-destruct[95].

Comparision study

The comparision study of AgNPs with the previous work is depected in Table 12 below.

Conclusion

In this study, *Discopodium Penninervium Hochst* leaf extract was employed to green synthesize silver nanoparticles (AgNPs) for antimicrobial activities. The RSM analysis result revealed the concentration of $AgNO_3$ significantly influences the size of AgNPs. The smallest particle size of 21.65 nm was obtained at the reaction temperature of

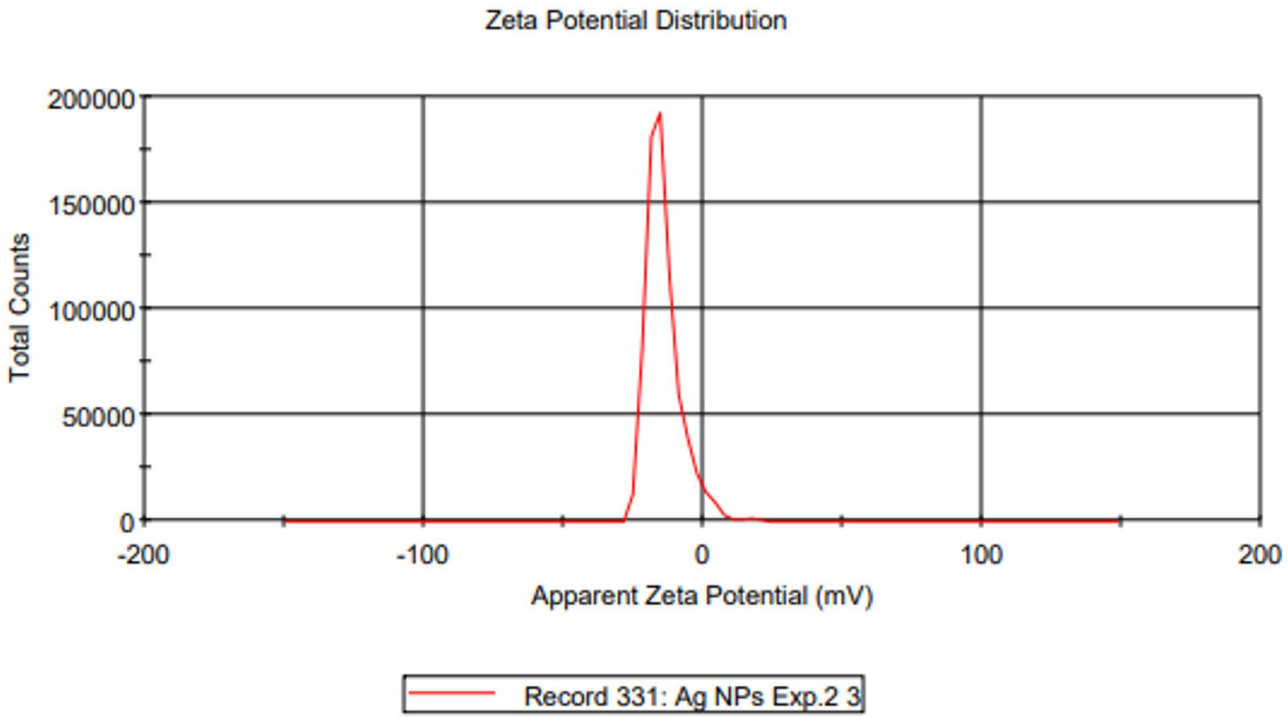

Fig. 14. Zeta potential analysis of silver nanoparticles (AgNPs).

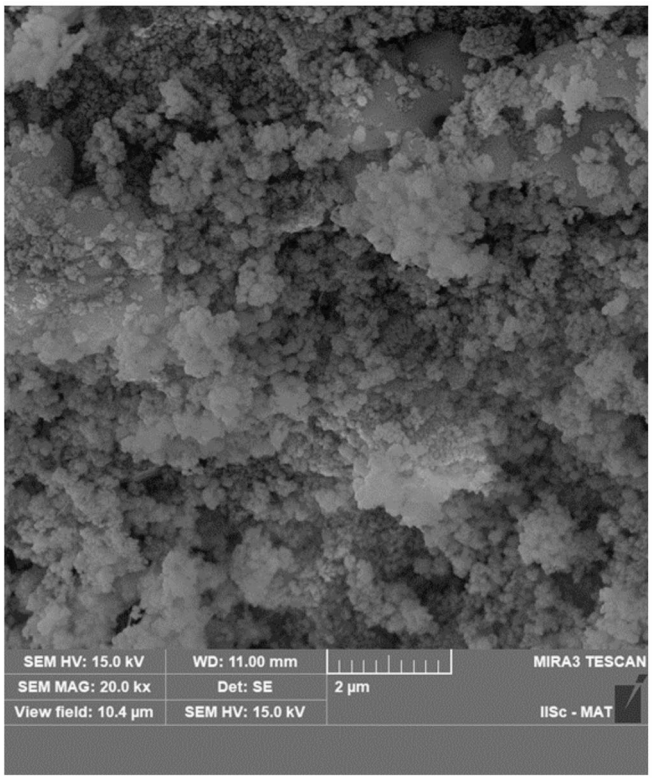

Fig. 15. SEM image of silver nanoparticles (AgNPs).

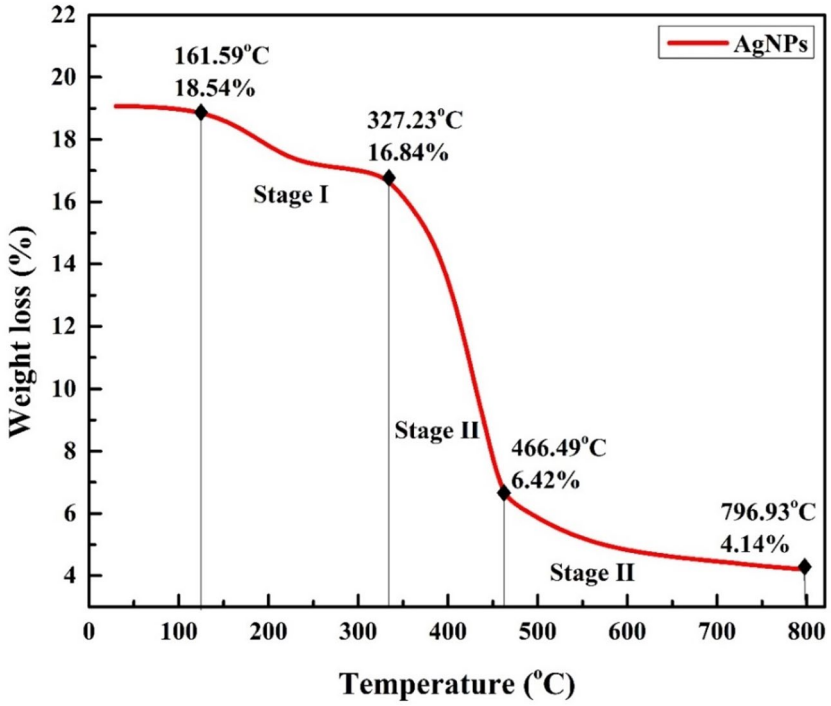

Fig. 16. TGA graph of silver nanoparticles (AgNPs).

81.06℃, pH of 11.49, and $AgNO_3$ concentration of 2.13 mM. Additionally, the physicochemical characterization studies of AgNPs were conducted by UV-Vis spectroscopy, XRD, FTIR, DLS, SEM, and TGA.

The UV-Vis spectra result revealed the sharp peak observed at a wavelength of 402 nm belongs to AgNPs, which demonstrated the proper synthesis of AgNPs. The XRD pattern exhibited the characteristic face-centered cubic (FCC) and an average crystallite size of 17.60 nm. FTIR analysis showed that AgNPs contain O −H, C −N, C −H, and C −Br functional groups, indicating their significant roles in the synthesis of AgNPs. The particle size distribution and zeta potential analysis by DLS exhibited an average particle size of 38.61 nm and a surface charge of 14.20 mV, respectively, which exhibit good stability of the synthesized AgNPs. SEM and TGA analysis revealed the synthesized AgNPs are spherical and exhibit good thermal stability. The synthesized AgNPs demonstrated effective antimicrobial activity against *E. coli*. Thus, this study presented simple, and eco-friendly methods for synthesizing AgNPs with potential antimicrobial applications. However, Gas chromatography Mass spectroscopy (GCMS) is recommended to investigate the concentration of bioactive compound in *Discopodium peninervum Hochst* leaf extract. To gain a better understanding of the thermal and physical properties of the synthesized AgNPs, techniques such as differential scanning calorimetry (DSC), energy dispersive spectroscopy (EDS), and transmission electron microscopy (TEM) analysis are recommended. Moreover, the leaf extract west management and cytotoxicity assessment of AgNPs and MBC are recommended for future studies.

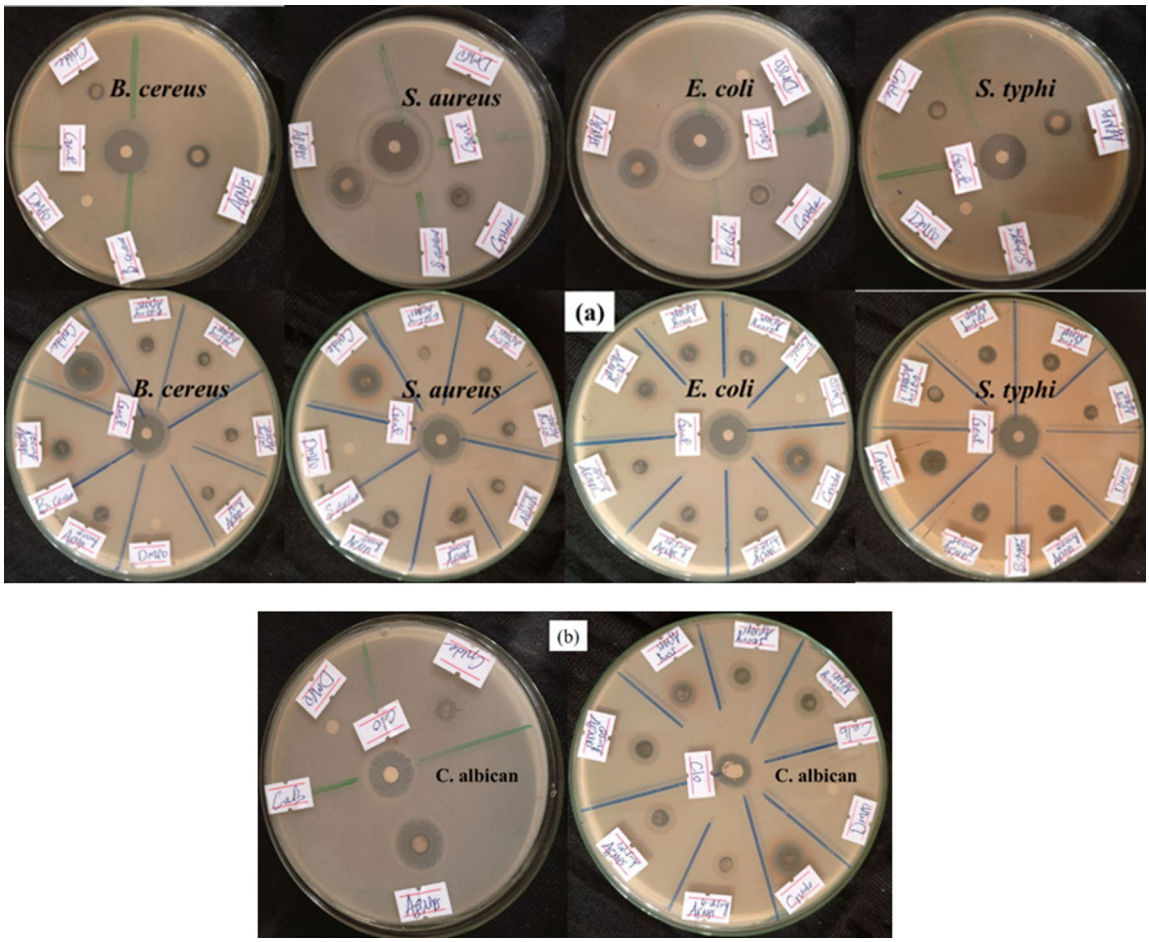

Fig. 17. Antibacterial (**a**) and antifungal (**b**) activities of silver nanoparticles (AgNPs) mediated *Discopodium Penninervium Hochst* leaf extract.

	Zone of inhibition (mm)						Gentamicin or Clotrimazole	DMSO	MIC (mg/mL)
	50 (mg/mL)	25 (mg/mL)	12.50 (mg/mL)	6.25 (mg/mL)	3.13 (mg/mL)	1.56 (mg/mL)			
B. cereus	14	11	10.75	9	8.25	7.25	22	-	0.78
S. aureus	21	12	10.50	9.50	8.75	8.25	25	-	0.40
E. coli	25	12.50	11.25	10.83	9.73	9.50	24	-	0.07
S. Typhi	13	10	9.50	8.25	8	7	24	-	1.56
C. albicans	20	16	14	13.5	13	9	20	-	0.20

Table 10. Evaluation of antibacterial and antifungal activities of silver nanoparticles (AgNPs).

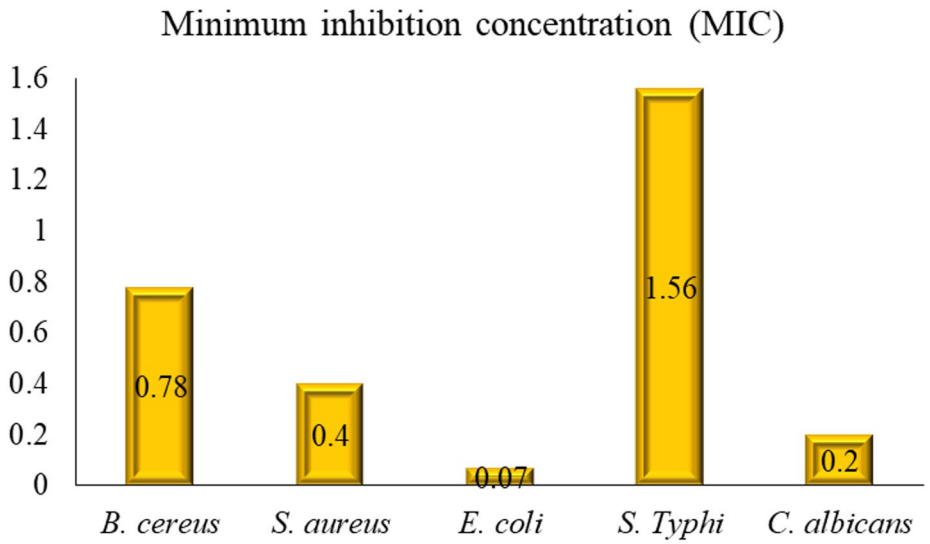

Fig. 18. Minimum inhibition concentration (MIC) of silver nanoparticles (AgNPs).

Average inhibition zone (mm)		
10.042	Mean (X)	11.68
11.667	Standard deviation (s)	2.07
13.135	Count (n)	5.00
9.292	Standard error mean (sem)	0.92
14.250	Degree of freedom (df)	4.00
	Hypothesized mean (μ)	0.2
	T- test	12.41
	P -value	0.00024

Table 11. T-test analysis of AgNPs againest antimicrobials.

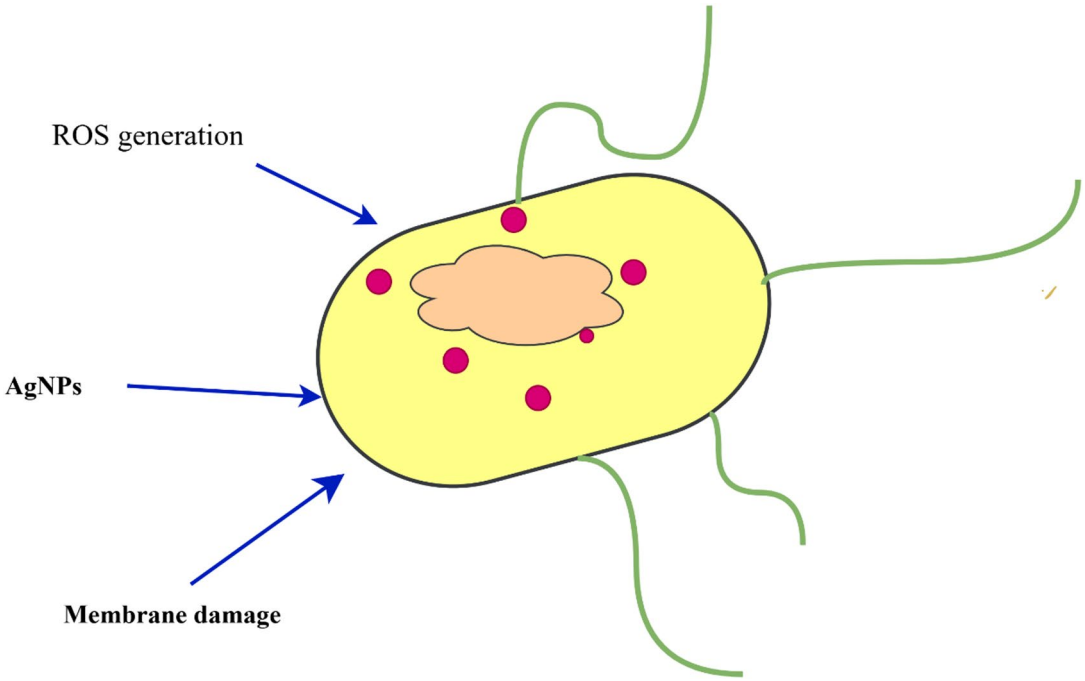

Fig. 19. Reactive oxygen species (ROS) mechanisim of antimicrobial activities of the synthesized silver nanoparticles (AgNPs).

Nonmaterial	Plant used	Microorganisms	Zone of inhibition	References
AgNPs	*Ginkgo Biloba* leaf extract	*S.aureus* *E. coli*	14 mm 18 mm	96
AgNPs	*Salvia sclarea L. (Clary Sage) flower extract*	*P. aeruginosa* *E. coli* *S.aureus* *B. cereus*	8.93 mm 10.46 mm 13.63 mm 15.13 mm	97
AgNPs	*Santalum album* Leaf extract	*S.aureus* *P. aeruginosa*	17.2 mm 12.3 mm	98
AgNPs	*Sida schimperiana Hochst* leaf extract	*E. coli* *K. Pneumonia* *S. aureus* *S. epidermidis*	26.33 mm 22 mm 23.33 mm 22.33 mm	99
AgNPs	*Discopodium Penninervium Hochst* leaf extract	*B. cereus* *S. aureus* *E. coli* *S. Typhi* *C. albicans*	14 mm 21 mm 25 mm 13 mm 20 mm	This study

Table 12. Comparison of antimicrobial activities of AgNPs.

Data availability

The data used in this study can be available from the corresponding authors at reasonable request.

Received: 4 September 2025; Accepted: 14 November 2025
Published online: 22 November 2025

References

1. Balestri, A., Cardellini, J. & Berti, D. Gold and silver nanoparticles as tools to combat multidrug-resistant pathogens. *Curr. Opin. Colloid Interface Sci.* **66**, 101710 (2023).
2. Thakur, M., Poojary, S. & Swain, N. Green synthesis of iron oxide nanoparticles and its biomedical applications. *Nanotechnol Life Sci.* **1** (1), 83–109. https://doi.org/10.1007/978-3-030-64410-9_5 (2021).
3. B. Mekuye and B. Abera, "Nanomaterials: An overview of synthesis, classification, characterization, and applications," Nano Sel., vol. 4, no. 8, pp. 486–501, 2023.
4. Zahin, N. et al. Nanoparticles and its biomedical applications in health and diseases: special focus on drug delivery. *Environ. Sci. Pollut Res.* **27**(16), 19151–19168 (2020).
5. G. Vijayakumar, H. J. Kim, and S. K. Rangarajulu, "In Vitro Antibacterial and Wound Healing Activities Evoked by Silver Nanoparticles Synthesized through Probiotic Bacteria," Antibiotics, vol. 12, no. 1, pp. 1–21, 2023, doi: 10.3390/antibiotics12010141.

6. Narayanan, K. B. & Bhaskar, R. Green nanotechnology: paving the way for environmental sustainability. *Sustain* **16**, 0–3. https://doi.org/10.3390/su16146262 (2024).
7. Hermosilla, E. et al. Synthesis of antimicrobial Chitosan-Silver nanoparticles mediated by reusable Chitosan fungal beads. *Int. J. Mol. Sci.* **24** (3). https://doi.org/10.3390/ijms24032318 (2023).
8. A. Sati et al., "Silver Nanoparticles (AgNPs) as potential antiviral agents: synthesis, biophysical properties, safety, challenges and future directions— update review," Molecules, vol. 30, no. 9, p. 2004, 2025.
9. Hashem, A. H. et al. Antifungal activity of biosynthesized silver nanoparticles (AgNPs) against aspergilli causing aspergillosis: ultrastructure study. *J. Funct. Biomater.* **13** (4), 242 (2022).
10. Gul, A. R. et al. Grass-mediated biogenic synthesis of silver nanoparticles and their drug delivery evaluation: A biocompatible anti-cancer therapy. *Chem. Eng. J.* **407**, 127202 (2021).
11. Kim, D. Y. et al. Development of novel peptide-modified silver nanoparticle-based rapid biosensors for detecting aminoglycoside antibiotics. *J. Agric. Food Chem.* **71** (34), 12883–12898 (2023).
12. Ahmed, B., Tahir, M. B., Sagir, M. & Hassan, M. Bio-inspired sustainable synthesis of silver nanoparticles as next generation of nanoproduct in antimicrobial and catalytic applications. *Mater. Sci. Eng. B.* **301**, 117165 (2024).
13. Sharma, D., Gulati, S. S., Sharma, N. & Chaudhary, A. Sustainable synthesis of silver nanoparticles using various biological sources and waste materials: A review. *Emergent Mater.* **5** (6), 1649–1678 (2022).
14. Bala, A. & Rani, G. A review on phytosynthesis, affecting factors and characterization techniques of silver nanoparticles designed by green approach. *Int. Nano Lett.* **10** (3), 159–176. https://doi.org/10.1007/s40089-020-00309-7 (2020).
15. Mustapha, T., Misni, N., Ithnin, N. R., Daskum, A. M. & Unyah, N. Z. A review on plants and microorganisms mediated synthesis of silver nanoparticles, role of plants metabolites and applications. *Int. J. Environ. Res. Public. Health.* **19** (2), 674 (2022).
16. Jaldurgam, F. F., Ahmad, Z. & Touati, F. Synthesis and performance of large-scale cost-effective environment-friendly nanostructured thermoelectric materials. *Nanomaterials* **11** (5), 1091 (2021).
17. Ying, S. et al. Green synthesis of nanoparticles: current developments and limitations. *Environ. Technol. Innov.* **26**, 102336. https://doi.org/10.1016/j.eti.2022.102336 (2022).
18. Kaur, N. et al. Lycium Shawii mediated green synthesis of silver nanoparticles, characterization and assessments of their phytochemical, antioxidant, antimicrobial properties. *Inorg. Chem. Commun.* **159**, 111735 (2024).
19. Ayalew, H. et al. Chemical composition and in vitro antileishmanial activity of essential oil of the leaves of discopodium pennnervium Hochst. *EPJ* **34** (2), 75–80 (2018).
20. Chandraker, S. K. et al. Biofabrication of spherical silver nanoparticles using leaf extract of plectranthus barbatus andrews: characterization, free radical scavenging, and optical properties. *Inorg. Chem. Commun.* **142**, 109669 (2022).
21. Bacha, E. G. Response Surface Methodology Modeling, Experimental Validation, and Optimization of Acid Hydrolysis Process Parameters for Nanocellulose Extraction, *South African J. Chem. Eng.*, vol. **40**, no. December pp. 176–185, 2022, (2021). https://doi.org/10.1016/j.sajce.2022.03.003
22. MuthuKathija, M., Badhusha, M. S. M. & Rama, V. Green synthesis of zinc oxide nanoparticles using Pisonia Alba leaf extract and its antibacterial activity. *Appl. Surf. Sci. Adv.* **15**, 100400 (2023).
23. Sharifi-Rad, M., Elshafie, H. S. & Pohl, P. Green synthesis of silver nanoparticles (AgNPs) by lallemantia Royleana leaf extract: their bio-pharmaceutical and catalytic properties. *J. Photochem. Photobiol Chem.* **448**, 115318 (2024).
24. Asif, M. et al. Green Synthesis of Silver Nanoparticles (AgNPs), Structural Characterization, and their Antibacterial Potential, *Dose-Response*, vol. 20, no. 1, pp. 1–11, (2022). https://doi.org/10.1177/15593258221088709
25. Velusamy, P., Das, J., Pachaiappan, R., Vaseeharan, B. & Pandian, K. Greener approach for synthesis of antibacterial silver nanoparticles using aqueous solution of Neem gum (Azadirachta indica L). *Ind. Crops Prod.* **66** (1), 103–109. https://doi.org/10.1016/j.indcrop.2014.12.042 (2015).
26. Sarwer, Q. et al. Green synthesis and characterization of silver nanoparticles using Myrsine Africana leaf extract for their Antibacterial, antioxidant and phytotoxic activities. *Molecules* **27**, 1–14. https://doi.org/10.3390/molecules27217612 (2022).
27. Satyavani, K., Ramanathan, T. & Gurudeeban, S. Green synthesis of silver nanoparticles by using stem derived callus extract of bitter Apple (Citrullus colocynthis). *Dig. J. Nanomater Biostructures.* **6** (3), 1019–1024 (2011).
28. Shankar, T., Karthiga, P., Swarnalatha, K. & Rajkumar, K. Green synthesis of silver nanoparticles using capsicum frutescence and its intensified activity against E. coli Resource-Efficient technologies green synthesis of silver nanoparticles using capsicum frutescence and its intensified activity against E. co. *Resour. Technol.* **3** (3), 303–308. https://doi.org/10.1016/j.reffit.2017.01.004 (2021).
29. Rajeshkumar, S. Synthesis of silver nanoparticles using fresh bark of Pongamia pinnata and characterization of its antibacterial activity against gram positive and gram negative pathogens. *Resour. Technol.* **2** (1), 30–35. https://doi.org/10.1016/j.reffit.2016.06.003 (2016).
30. Sathishkumar, M. et al. Cinnamon zeylanicum bark extract and powder mediated green synthesis of nano-crystalline silver particles and its bactericidal activity. *Colloids Surf. B Biointerfaces.* **73** (2), 332–338. https://doi.org/10.1016/j.colsurfb.2009.06.005 (2009).
31. Sharma, N. et al. Preparation and evaluation of the ZnO NP–ampicillin/sulbactam nanoantibiotic: optimization of formulation variables using RSM coupled GA method and antibacterial activities. *Biomolecules* **9** (12), 1–17. https://doi.org/10.3390/biom9120764 (2019).
32. Teka, A., Asfaw, Z., Demissew, S. & Van Damme, P. Traditional medicinal plant use of Indigenous communities in gurage zone, Ethiopia. *Ethnobot Res. Appl.* **19**, 1–31. https://doi.org/10.32859/ERA.19.41.1-31 (2020).
33. Teka, A., Asfaw, Z., Demissew, S. & Van Damme, P. Medicinal-plant-use- (2020). practice-in-four-ethnic-communities-Gurage-Mareqo-Qebena-and-Silti-south-central-EthiopiaJournal-of-Ethnobiology-and-Ethnomedicine.pdf, vol. 1, pp. 1–12.
34. Dahal, S. & Heinen, J. T. A history of the convention on international trade in endangered species of wild fauna and flora implementation in Nepal. *Diversity* **17** (5), 312 (2025).
35. G. Shrivastav, T. Prava Jyoti, S. Chandel, and R. Singh, "Eco-friendly extraction: innovations, principles, and comparison with traditional methods," Sep. Purif. Rev., vol. 54, no. 3, pp. 241–257, 2025.
36. Melkamu, W. W. & Bitew, L. T. Green synthesis of silver nanoparticles using Hagenia abyssinica (Bruce) J.F. Gmel plant leaf extract and their antibacterial and anti-oxidant activities. *Heliyon* **7** (11), e08459. https://doi.org/10.1016/j.heliyon.2021.e08459 (2021).
37. M. Rutkowski, L. Krzemińska-Fiedorowicz, K. Khachatryan, G. Khachatryan, A. Kalisz, and A. Sękara, "Impact of silver nanoparticles in alginate gels on seed germination, growth and stress biochemical parameters of cucumber seedlings," Plant Stress, vol. 12, p. 100491, 2024
38. Adewale, A., Ifeoluwa, A. P., Olusoji, O. A., Bukunmi, A. A. & Simeon, O. O. Historical, botanical and medicinal perspectives on ginger (Zingiber officinale). *J. Complement. Altern. Med. Res.* **15**, 44–67 (2021).
39. Obi, P. U. et al. Analysis of Proximate, mineral and phytochemical composition of fresh and dry Vernonia amygdalina (Bitter Leaf) in Bida Metropolis, Niger state. *UMYU Sci.* **3** (1), 88–94 (2024).
40. Chirumamilla, P., Dharavath, S. B. & Taduri, S. Eco-friendly green synthesis of silver nanoparticles from leaf extract of solanum khasianum: optical properties and biological applications. *Appl. Biochem. Biotechnol.* **195** (1), 353–368 (2023).
41. Sy Mohamad, S. F. et al. Application of experimental designs and response surface methods in screening and optimization of reverse micellar extraction. *Crit. Rev. Biotechnol.* **40** (3), 341–356 (2020).
42. Gowda, A., TC, S., Anil, V. S. & Raghavan, S. Phytosynthesis of silver nanoparticles using aqueous sandalwood (Santalum album L.) leaf extract: divergent effects of SW-AgNPs on proliferating plant and cancer cells. *PLoS One.* **19** (4), e0300115 (2024).

43. Chinnasamy, R. et al. Phyto-fabrication of AgNPs using leaf extract of vitex trifolia: potential to antibacterial, antioxidant, dye degradation, and their evaluation of non-toxicity to chlorella vulgaris. *Biomass Convers. Biorefinery*. **14** (13), 14903–14920 (2024).
44. Ansari, N. et al. Green synthesis of nanomaterials: properties and their potential applications. *Sci. Adv. Mater.* **16** (8), 837–854 (2024).
45. A. M. Sivalingam et al., "Extraction, biosynthesis, and characterization of silver nanoparticles for its enhanced applications of antibacterial activity using the Silybum marianum Linn. plant," Biomass Convers. Biorefinery, vol. 14, no. 23, pp. 30227–30238, 2024.
46. Khan, F. et al. Green nanotechnology: Plant-Mediated nanoparticle synthesis and application. *Nanomaterials* **12** (4). https://doi.org/10.3390/nano12040673 (2022).
47. Akintelu, S. A., Bo, Y. & Folorunso, A. S. A review on synthesis, optimization, mechanism, characterization, and antibacterial application of silver nanoparticles synthesized from plants, *J. Chem.*, vol. pp. 1–12, 2020. (2020).
48. Hossain, M. M., Mok, Y. S. & Wu, S. Investigation of silver nanoparticle synthesis with various nonthermal plasma reactor configurations. *Arab. J. Chem.* **16** (10), 105174 (2023).
49. I. Ahmad et al., "Application of central composite design for optimizing and statistical analysis of ultrasound-assisted removal of dyes from aqueous solution," Front. Environ. Sci., vol. 13, p. 1622134, 2025.
50. Yiğit, U. & Türkkan, M. Antifungal activity and optimization procedure of microwave-synthesized silver nanoparticles using Linden (Tilia rubra subsp. caucasica) flower extract. *Int. J. Chem. Technol.* **7** (1), 25–37 (2023).
51. Kayhomayoon, Z. et al. A combination of metaheuristic optimization algorithms and machine learning methods improves the prediction of groundwater level. *Water* **14** (5), 751 (2022).
52. Klein, J. et al. Limitations of the Tauc plot method. *Adv. Funct. Mater.* **33** (47), 2304523 (2023).
53. Balaji, V. et al. Bio-inspired synthesis of silver nanoparticles and their nanocomposites for antibacterial and anticancer activity: a comparative study. *J. Alloys Compd.* **966**, 171503 (2023).
54. Parvathalu, K. et al. Green synthesis of silver nanoparticles using argyreia nervosa leaf extract and their antimicrobial activity. *Plasmonics* **18** (3), 1075–1081 (2023).
55. N. D. Radnović et al., "Synthesis, Characterization, and Impact of Water on the Stability of Postmodified Schiff Base Containing Metal–Organic Frameworks," Inorganics, vol. 11, no. 11, p. 432, 2023.
56. Chen, Y. et al. Involvement of Acid-Leachable inorganics in pyrolysis of pig manure. *Energy Fuels*. **38** (14), 13039–13049 (2024).
57. Singha, K., Kumari, G., Jagadevan, S., Sarkar, A. N. & Pal, S. In situ synthesis of exfoliated Ni (OH) 2 nanosheets and AgNPs-Embedded functionalized Polyindole-Based trinary hybrid microspheres: A Z-Scheme photocatalyst for the Sunlight-Driven degradation of organic pollutants with enhanced antibacterial efficacy. *Langmuir* **40** (31), 16208–16225 (2024).
58. Xiang, L. et al. Block copolymer self-assembly directed synthesis of porous materials with ordered bicontinuous structures and their potential applications. *Adv. Mater.* **35** (5), 2207684 (2023).
59. Chuang, Z. et al. Minimum false-positive risk of primary outcomes and impact of reducing nominal P-value threshold from 0.05 to 0.005 in anaesthesiology randomised clinical trials: a cross-sectional study. *Br. J. Anaesth.* **130** (4), 412–420 (2023).
60. Rose, P. K. et al. Congo red dye removal using modified banana leaves: adsorption equilibrium, kinetics, and reusability analysis. *Groundw. Sustain. Dev.* **23**, 101005 (2023).
61. N. Maleki, O. Lundström, A. Musaddiq, J. Jeansson, T. Olsson, and F. Ahlgren, "Future energy insights: Time-series and deep learning models for city load forecasting," Appl. Energy, vol. 374, p. 124067, 2024.
62. Ripanda, A. et al. Optimizing Ciprofloxacin removal from water using Jamun seed (Syzygium cumini) biochar: A sustainable approach for ecological protection. *HydroResearch* **7**, 164–180 (2024).
63. Wasilewska, A. et al. Physico-chemical properties and antimicrobial activity of silver nanoparticles fabricated by green synthesis. *Food Chem.* **400**, 133960 (2023).
64. Chen, Y., Peng, Y., Guo, Q. & Qin, J. Raman enhancement effect of different Au@ ag NPs on S. Typhi. *Sens. Agric. Food Qual. Saf. XV*. **12545**, 93–102 (2023).
65. Sun, M. et al. Enhanced Anti-Inflammatory activity of Tilianin based on the novel amorphous nanocrystals. *Pharmaceuticals* **17** (5), 654 (2024).
66. [1] N. P. U. Nguyen, N. T. Dang, L. Doan, and T. T. H. Nguyen, "Synthesis of silver nanoparticles: from conventional to 'modern'methods—a review," Processes, vol. 11, no. 9, p. 2617, 2023.
67. Gherbi, B. et al. Effect of pH value on the bandgap energy and particles size for biosynthesis of ZnO nanoparticles: efficiency for photocatalytic adsorption of Methyl orange. *Sustain* **14** (18). https://doi.org/10.3390/su141811300 (2022).
68. Nguyen, N. P. U., Dang, N. T., Doan, L. & Nguyen, T. T. H. Synthesis of silver nanoparticles: from conventional to 'modern'methods—a review. *Processes* **11** (9), 2617 (2023).
69. Duraisamy, R., Arizo, A. & Yilma, B. Antibacterial and antioxidant activity of plant-mediated green synthesized silver nanoparticles using Cissus quadrangularis aqueous extract. *Bull. Chem. Soc. Ethiop.* **39** (3), 483–502 (2025).
70. Soo, X. Y. D. et al. Hydrolytic degradation and biodegradation of polylactic acid electrospun fibers. *Chemosphere* **350**, 141186 (2024).
71. Zhang, S. et al. Preparation of ultrafine and highly loaded silver nanoparticle composites and their highly efficient applications as reductive catalysts and antibacterial agents. *J. Colloid Interface Sci.* **629**, 766–777 (2023).
72. Wu, Z. et al. Investigating the effect of pH on the growth of coprecipitated Ni0. 8Co0. 1Mn0. 1 (OH) 2 agglomerates as precursors of cathode materials for Li-ion batteries. *Ceram. Int.* **49** (10), 15851–15864 (2023).
73. Khan, J. et al. Green synthesis of silver nanoparticles (Ag-NPs) using debregeasia salicifolia for biological applications. *Mater. (Basel)*. **16** (1). https://doi.org/10.3390/ma16010129 (2023).
74. Hermosilla, E. et al. Molecular weight identification of compounds involved in the fungal synthesis of agnps: effect on antimicrobial and photocatalytic activity. *Antibiotics* **11** (5). https://doi.org/10.3390/antibiotics11050622 (2022).
75. Reda, M. et al. Green synthesis of potent antimicrobial silver nanoparticles using different plant extracts and their mixtures, *Processes*, vol. 7, no. 8, (2019). https://doi.org/10.3390/pr7080510
76. Alemu, T. A. et al. Highly sensitive detection of bacteria (E. Coli) endotoxin using novel PANI-benzimidazole-Ag nanocomposite by DMMB dye displacement assay. *Mater. Res. Express*. **10** (7), 75302 (2023).
77. Chandraker, S. K., Lal, M. & Shukla, R. DNA-binding, antioxidant, H2O2 sensing and photocatalytic properties of biogenic silver nanoparticles using: ageratum conyzoides L. leaf extract. *RSC Adv.* **9** (40), 23408–23417. https://doi.org/10.1039/c9ra03590g (2019).
78. Gharari, Z., Hanachi, P., Sadeghinia, H. & Walker, T. R. Cichorium intybus bio-callus synthesized silver nanoparticles: A promising antioxidant, antibacterial and anticancer compound. *Int. J. Pharm.* **625**, 122062 (2022).
79. Mani, M. et al. Studies on the spectrometric analysis of metallic silver nanoparticles (Ag NPs) using Basella Alba leaf for the antibacterial activities. *Environ. Res.* **199, no.** https://doi.org/10.1016/j.envres.2021.111274 (May, 2021).
80. Barik, B., Satapathy, B. S., Pattnaik, G., Bhavrao, D. V. & Shetty, K. P. Sustainable synthesis of silver nanoparticles from Azadirachta indica: antimicrobial, antioxidant and in silico analysis for periodontal treatment, *Front. Chem.*, vol. 12, no. October, pp. 1–14, (2024). https://doi.org/10.3389/fchem.2024.1489253
81. N. Stozhko, A. Tarasov, V. Tamoshenko, M. Bukharinova, E. Khamzina, and V. Kolotygina, "Green silver nanoparticles: Plant-extract-mediated synthesis, optical and electrochemical properties," Physchem, vol. 4, no. 4, pp. 402–419, 2024.
82. Velgosova, O., Dolinská, S., Podolská, H., Mačák, L. & Čižmárová, E. Impact of plant extract phytochemicals on the synthesis of silver nanoparticles. *Mater. (Basel)*. **17** (10). https://doi.org/10.3390/ma17102252 (2024).

83. Singh, P. K., Singh, J., Medhi, T. & Kumar, A. Phytochemical Screening, Quantification, FT-IR Analysis, and In Silico Characterization of Potential Bio-active Compounds Identified in HR-LC/MS Analysis of the Polyherbal Formulation from Northeast India., *ACS omega*, vol. 7, no. 37, pp. 33067–33078, Sep. (2022). https://doi.org/10.1021/acsomega.2c03117
84. Hoseini, B. et al. Application of ensemble machine learning approach to assess the factors affecting size and polydispersity index of liposomal nanoparticles. *Sci. Rep.* **13** (1), 18012 (2023).
85. Balamurugan, V., Ragavendran, C. & Arulbalachandran, D. Eco-friendly green synthesis of AgNPs from Elaeocarpus serratus fruit extract: potential to antibacterial, antioxidant, cytotoxic effects of colon cancerous cells (HT-29) and its toxicity assessments of marine microcrustacean artemia nauplii. *Mol. Biol. Rep.* **51** (1), 418 (2024).
86. Mohammed, I. et al. Effect of sulfate-based scales on calcite mineral surface chemistry: insights from zeta-potential experiments and their implications on wettability. *ACS Omega*. **7** (32), 28571–28587 (2022).
87. Hayat, P. et al. Myogenesis and Analysis of Antimicrobial Potential of Silver Nanoparticles (AgNPs) against Pathogenic Bacteria,., (2023).
88. Gharari, Z., Hanachi, P., Sadeghinia, H. & Walker, T. R. Eco-Friendly green synthesis and characterization of silver nanoparticles by scutellaria multicaulis leaf extract and its biological activities. *Pharmaceuticals* **16** (7). https://doi.org/10.3390/ph16070992 (2023).
89. Moteriya, P. & Chanda, S. Green synthesis of silver nanoparticles from caesalpinia pulcherrima leaf extract and evaluation of their antimicrobial, cytotoxic and genotoxic potential (3-in-1 system). *J. Inorg. Organomet. Polym. Mater.* **30**, 3920–3932 (2020).
90. Lacerda, D. et al. Antibacterial and antibiofilm potential of silver nanoparticles against antibiotic-sensitive and multidrug-resistant Pseudomonas aeruginosa strains, *Brazilian J. Microbiol.*, vol. 52, pp. 267–278, [Online]. (2021). Available: https://doi.org/10.1007/s42770-020-00406-x
91. Khire, T. S. et al. Rapid minimum inhibitory concentration (MIC) analysis using lyophilized reagent beads in a novel Multiphase, Single-Vessel assay. *Antibiotics* **12** (11). https://doi.org/10.3390/antibiotics12111641 (2023).
92. Parvekar, P., Palaskar, J., Metgud, S., Maria, R. & Dutta, S. The minimum inhibitory concentration (MIC) and minimum bactericidal concentration (MBC) of silver nanoparticles against Staphylococcus aureus. *Biomater. Investig Dent.* **7** (1), 105–109 (2020).
93. Venditti, P. & Meo, S. D. The role of reactive oxygen species in the life cycle of the mitochondrion. *Int. J. Mol. Sci.* **21** (6), 2173 (2020).
94. Chandraker, S. K. & Kumar, R. Biogenic biocompatible silver nanoparticles: a promising antibacterial agent. *Biotechnol. Genet. Eng. Rev.* **40** (4), 3113–3147 (2024).
95. C. A. Juan, J. M. Pérez de la Lastra, F. J. Plou, and E. Pérez-Lebeña, "The chemistry of reactive oxygen species (ROS) revisited: outlining their role in biological macromolecules (DNA, lipids and proteins) and induced pathologies," Int. J. Mol. Sci., vol. 22, no. 9, p. 4642, 2021.
96. Mohamed, A., Dayo, M., Alahmadi, S. & Ali, S. Anti-Inflammatory and antimicrobial activity of silver nanoparticles Green-Synthesized using extracts of different plants. *Nanomaterials* **14** (17). https://doi.org/10.3390/nano14171383 (2024).
97. Zarei, Z., Razmjoue, D., Moazeni, M., Azarnivand, H. & Oroojalian, F. Salvia sclarea L.(Clary Sage) flower extract-mediated green synthesis of silver nanoparticles and their characterization, antibacterial, antifungal, and scolicidal activities against Echinococcus granulosus. *Microbe* **5**, 100216 (2024).
98. Selvam, K., Sudhakar, C. & Prasath, A. R. Green synthesis and characterization of silver nanoparticles from sandalwood (Santalum album L.) extract for efficient catalytic reduction, antioxidant and antibacterial activity. *Biocatal. Agric. Biotechnol.* **57**, 103094 (2024).
99. Moges, W. & Misskire, Y. Green synthesis, characterization and antibacterial activities of silver nanoparticles using Sida schimperiana Hochst. Ex A. Rich (Chifrig) leaves Extract. *Discov Mater.* **5** (1), 34 (2025).

Acknowledgements

The authors gratefully acknowledge the School of Chemical Engineering and the Faculty of Materials Science and Engineering for generously granting us access to the laboratory facilities and resources to conduct the research work. The authors also acknowledge JiT Center of Excellence for partial support of this work.

Author contributions

Abreham Mulugeta Getachew conceptualized, Investigated, analyzed data, writing-original draft, writing-review & editing. Ebise Getacho Bacha conceptualized, writing-original draft, writing-review & editing, and supervised the research work. Wondwosen Sime Geleta conceptualized, writing-original draft, writing-review & editing,, and supervised the research work.

Funding

This research received no external funding.

Declarations

Competing interests

The authors declare no competing interests.

Consent for publication

All authors have consented to the publication of this article.

Additional information

Supplementary Information The online version contains supplementary material available at https://doi.org/10.1038/s41598-025-29253-2.

Correspondence and requests for materials should be addressed to A.M.G.